The Integrated "Multiomics" Landscape at Peak Injury and Resolution From Alcohol-Associated Liver Disease

Sukanta Das,[1] Xiaodong Ge,[1] Hui Han,[1] Romain Desert,[1] Zhuolun Song (iD) ,[1] Dipti Athavale,[1] Wei Chen,[1] Harriet Gaskell,[1] Daniel Lantvit,[1] Grace Guzman,[1] and Natalia Nieto (iD) [1,2]

Alcohol-associated liver disease (ALD) is a significant clinical problem for which the most effective therapy is alcohol abstinence. The two aims of this study were, first, to identify the liver transcriptome, fecal microbiome, and portal serum metabolome at peak injury and during early and late resolution from ALD; and second, to integrate their interactions and understand better the pathogenesis of ALD. To provoke alcohol-induced liver injury, female and male wild-type mice were fed the control or ethanol Lieber-DeCarli diets for 6 weeks. To study early and late resolution, alcohol was withdrawn from the diet and mice were sacrificed after 3 and 14 days, respectively. At peak injury, there was increased signal transducer and activator of transcription (*Stat3*), *Rho-GTPases*, *Tec kinase* and glycoprotein VI (*Gp6*), and decreased peroxisome proliferator–activated receptor signaling. During resolution from ALD, there was up-regulation of vitamin D receptor/retinoid X receptor, toll-like receptor, *p38* and *Stat3*, and down-regulation of liver X receptor signaling. Females showed significant changes in catabolic pathways, whereas males increased cellular stress, injury, and immune-response pathways that decreased during resolution. The bacterial genus *Alistipes* and the metabolite dipeptide glycyl-L-leucine increased at peak but decreased during resolution from ALD in both genders. Hepatic induction of mitogen-activated protein kinase (*Map3k1*) correlated with changes in the microbiome and metabolome at peak but was restored during ALD resolution. Inhibition of MAP3K1 protected from ALD in mice. *Conclusion:* Alcohol abstinence restores the liver transcriptome, fecal microbiome, and portal serum metabolome in a gender-specific manner. Integration of multiomics data identified *Map3k1* as a key gene driving pathogenesis and resolution from ALD. (*Hepatology Communications* 2022;6:133-160).

A ccording to the National Institutes on Alcohol Abuse and Alcoholism, about 88,000 people (62,000 men and 26,000 women) die from alcohol use disorders annually, making alcohol the third leading preventable cause of death in the United States. Overall, alcohol causes more than 5% of the global disease burden worldwide.

Alcohol and the by-products of its metabolism play a central hepatotoxic role in alcohol-associated liver disease (ALD).[1,2] The precise molecular mechanisms driving the onset of simple fatty liver disease and progression to hepatocellular carcinoma due to alcohol consumption are not completely elucidated.[1,3] Nevertheless, alcohol affects hepatic global gene expression.[4-7]

Chronic alcohol abuse also disrupts the intestinal epithelial barrier, decreases transepithelial electric resistance, and increases gut permeability.[8] These events enable gut-derived bacteria, bacterial products, such as lipopolysaccharide (LPS) and antigens, to translocate from the gut lumen to the portal vein. After reaching the liver, they activate Kupffer cells and infiltrating macrophages to eventually trigger hepatocyte injury.[8-10]

In addition, alcohol and its metabolite acetaldehyde cause bacterial overgrowth and intestinal dysbiosis,[11-13] both of which affect key metabolic pathways along with the composition of the bile acid (BA) pool, contributing to the ALD progression.[14]

To date, there is limited information on how ALD progresses and, more importantly, when and how it resolves. Therefore, the two aims of this study were, first, to identify the liver transcriptome, fecal microbiome, and portal serum metabolome at peak injury and during early and late resolution from ALD; and second, to integrate their interactions to understand better the pathogenesis of ALD.

Materials and Methods

GENERAL METHODOLOGY

Details on general methodology, such as hematoxylin and eosin (H&E) staining, measurement of serum alanine aminotransferase (ALT) and aspartate aminotransferase (AST) activities, serum and liver triglycerides (TGs) and cholesterol (CHO) concentration, serum alcohol levels, measurement of fluorescein isothiocyanate (FITC)–dextran in portal blood serum, total RNA extraction, and quantitative real-time polymerase-chase reaction (PCR) analysis are described in previous publications.[15-20] The sequences of the primers used are listed in Supporting Table S1. Immunohistochemistry (IHC) for MAP3K1 was performed using the PA5-79629 antibody (Invitrogen, Carlsbad, CA). IHC reactions were developed using the Histostain Plus detection system (Thermo Fisher Scientific, Carlsbad, CA). The same antibody was used for western blot (WB) analysis.

HUMAN SAMPLES

Tissue samples for WB analysis were provided by Dr. Zhaoli Sun from the Clinical Resources Center for Alcoholic Hepatitis Investigation (Johns Hopkins University, Baltimore, MD). The procurement and use of these archived samples was internal review board–approved.

MICE

C57BL/6J (Stock No. 000664) wild-type (WT) female and male mice were purchased from the Jackson Laboratory (Bar Harbor, ME).

MODEL OF ALCOHOL-INDUCED LIVER INJURY

The Lieber-DeCarli (LDC) model was used to provoke early alcohol-induced liver injury.[21] The control and ethanol LDC diets (Bio-Serv Inc., Frenchtown, NJ)

ARTICLE INFORMATION:

From the [1]Department of Pathology, University of Illinois at Chicago, Chicago, IL, USA; [2]Department of Medicine, Division of Gastroenterology and Hepatology, University of Illinois at Chicago, Chicago, IL, USA.

ADDRESS CORRESPONDENCE AND REPRINT REQUESTS TO:

Natalia Nieto, Pharm.D., Ph.D.
Department of Pathology, University of Illinois at Chicago
840 S. Wood St., Suite 130 CSN, MC 847

Chicago, IL 60612, USA
E-mail: nnieto@uic.edu
Tel.: +1- 312- 996- 7316

are equicaloric and have the same composition of fat (42% of calories) and protein (16% of calories). The content of carbohydrates is 42% of total calories (dextrin-maltose) in the control diet and 12% of total calories in the ethanol diet, where up to 30% of carbohydrate calories are replaced by ethanol.[21]

Equal number of female and male mice (12-week-old, ~25 g) were acclimatized to the liquid diet by feeding them the control LDC diet for 7 days. The percentage of ethanol-derived calories was progressively increased from 10% (1 week) to 20% (1 week), 25% (2 weeks) and 30% (2 weeks) to achieve peak injury. Resolution from ALD was develop by switching mice to control diet for 3 days (early resolution) or 14 days (late resolution). Control groups, at each time point, consisted of mice fed control LDC diet (Supporting Fig. S1A,B). Mice were pair-fed, and liver and body weight were recorded upon sacrifice to calculate the liver–to–body weight ratio. Blood was drawn by submandibular and portal vein bleeding under anesthesia. Feces were collected from the large intestine, and livers were removed.

MAP3K1 INHIBITION

MAP3K1 activity was inhibited by using phenethyl isothiocyanate (PEITC), which directly binds to the adenosine triphosphate binding pocket of MAP3K1 and results in inhibition of kinase activity.[22] PEITC (96%) was purchased from Thermo Fisher Scientific (Fair Lawn, NJ) and incorporated into the LDC diets. WT (12-week-old) female and male mice were allowed to acclimatize to the LDC liquid diet and then were randomly assigned into six groups (n = 4/group) and fed as follows: (1) LDC control diet for 6 weeks (control), (2) LDC control diet with 100 mg/kg/day PEITC for 6 weeks (control + PEITC), (3) LDC ethanol diet for 6 weeks (EtOH), (4) LDC ethanol diet with 100 mg/kg/day PEITC for 6 weeks (EtOH + PEITC), (5) LDC ethanol diet for 6 weeks followed by 3 days for LDC control (resolution), and (6) LDC ethanol diet for 6 weeks followed by 3 days for LDC control with 100 mg/kg/day PEITC (resolution + PEITC). The percentage of ethanol-derived calories was progressively increased as described before. Body weight was monitored weekly, and after 6 weeks or 6 weeks and 3 days of feeding, mice were sacrificed under anesthesia.

STIMULATION TO PRIMARY HEPATOCYTES

Primary hepatocytes from 12-week-old male WT mice were isolated and cultured in 12 well-plates (1×10^6 cells/well) as previously.[17] After 4 hours, hepatocytes were serum-deprived and treated with ethanol (100 mM), PEITC (20 µM), arachidonic acid (20 µM), LPS (1 µg/ml), tumor necrosis factor α (TNFα; 15 ng/mL), interleukin (IL)-1β (25 ng/mL), and H_2O_2 (1 µM) for 24 hours, and RNA and protein were isolated. Cytosolic and nuclear proteins were isolated using the compartmental protein extraction kit (Millipore, Burlington, MA).

STUDY APPROVAL

All animals received humane care according to the criteria outlined in the "Guide for the Care and Use of Laboratory Animals" prepared by the National Academy of Sciences and published by the National Institutes of Health. Housing and husbandry conditions were approved by the Institutional Animal Care and Use Committee office from the University of Illinois at Chicago before initiation of the studies. All *in vivo* experiments were carried out according to the Animal Research: Reporting of In Vivo Experiments guidelines.

STATISTICAL ANALYSIS

Data are given as means ± SEM unless otherwise indicated. Statistical analyses were performed using GraphPad Prism v7 with statistical significance set at $P \leq 0.05$. Comparisons between two groups were performed using the unpaired (two-tail) Student t test or Mann-Whitney U test.

Details methods are includes in the Supporting Information.

Results

LIVER INJURY AT PEAK AND RESOLUTION FROM ALD

WT mice were fed the control or ethanol LDC diets for 6 weeks to develop peak ALD. A separate group of mice with peak ALD was switched to

control diet for 3 or 14 days to allow early or late resolution, respectively. Liver injury was assessed by H&E staining, pathological scoring, and serum ALT activity. Both females and males at peak ALD showed increased steatosis, hepatocyte ballooning degeneration, and inflammation (Fig. 1A-E) as well as elevated ALT activity (Fig. 1F) compared with controls. In this model, inflammation results from proliferation and activation of Kupffer cells and infiltrating macrophages.[18] All of these parameters decreased significantly throughout resolution from ALD (Fig. 1A-F).

During progression to peak ALD, ethanol-fed mice showed lower body weight than control-fed mice, especially females. Throughout resolution from ALD, mice increased body weight, especially males (Supporting Fig. S1C,D). Liver weight and the liver–to–body weight ratio at peak ALD were significantly higher than in control-fed mice (Supporting Fig. S2A,B). Liver TGs and CHO, as well as serum ALT and AST activities, increased at peak ALD compared with controls, but decreased to baseline values during resolution (Supporting Fig. S2A,B and Fig. 1F). Overall, these findings suggest that ceasing alcohol consumption gradually resolves ALD.

LIVER TRANSCRIPTOME AT PEAK AND RESOLUTION FROM ALDLIVER TRANSCRIPTOME AT PEAK AND RESOLUTION FROM ALD

To examine the changes in hepatic gene expression occurring at peak and resolution from ALD, we performed RNA sequencing (RNA-seq). Both genders showed a large number of genes up-regulated (fold change (FC) ≥ 1.5) or down-regulated (FC ≤ 0.67) at peak and resolution from ALD (Fig. 2A-D). Further analysis revealed that nine genes in females and 1,057 genes in males increased at peak were down-regulated throughout resolution from ALD (Fig. 2A,C). Conversely, 16 genes in females and 1,208 genes in males decreased at peak were up-regulated throughout resolution from ALD (Fig. 2B,D). These results indicate that only 2.5% (25 of 970) genes in females return to baseline values throughout resolution from ALD as opposed to 46.5% (2,265 of 4,871) genes in males.

LANDSCAPE OF CANONICAL PATHWAYS AT PEAK AND RESOLUTION FROM ALD

Next, using Ingenuity Pathway Analysis (IPA), we analyzed the transcriptomics data to identify canonical pathways changing at peak and resolution from ALD. Females had a significant number of pathways changed at peak ALD (Fig. 3A,B). Among the activated, only STAT3 and death receptor signaling decreased during late resolution from ALD (Fig. 3A). Among the inactivated, only LPS/IL-1 mediated inhibition of retinoid X receptor (RXR) signaling increased throughout resolution from ALD (Fig. 3B). Peroxisome proliferator–activated receptor (PPAR) signaling, suppressed at peak, was reactivated during late resolution from ALD (Fig. 3B). Activation of serotonin catabolism at peak was reduced in early resolution from ALD (Fig. 3C). The genes from these pathways are listed in Supporting Table S2.

Males showed a remarkable number of changed pathways at peak injury (Fig. 3D,E). Among the activated, seven decreased throughout resolution from ALD (Fig. 3D). Endothelial growth factor (EGF) and fibroblast growth factor (FGF), as well as relaxin and Rho family of GTPases (Rho-GTPases) signaling, decreased during early and late resolution from ALD, respectively (Fig. 3D). Of note, STAT3 signaling remained activated in males (Fig. 3D) but not in females (Fig. 3A). Among the inactivated, eight pathways increased throughout resolution from ALD (Fig. 3E). PPAR, neurotrophin/TRK, and angiopoietin signaling were activated in early resolution from ALD (Fig. 3E). Three activated pathways associated with cellular stress and injury (acute phase response, coagulation, and reactive oxygen species [ROS]/reactive nitrogen species [RNS]) and four pathways linked to the immune response (IL-6, IL-8, IL-1, and dendritic cell maturation) at peak were reduced during resolution from ALD (Fig. 3F). The genes from these pathways are listed in Supporting Table S3.

COMMON GENES IN PATHWAYS CHANGED AT PEAK AND RESTORED THROUGHOUT RESOLUTION FROM ALD

There were 15 genes in females and 40 in males linked with multiple pathways changed at peak and

FIG. 1. Liver injury at peak and resolution from ALD. Female and male WT mice were fed the control or ethanol LDC diets for 6 weeks (peak injury). To achieve resolution from ALD, mice were switched to control diet for 3 or 14 days (early or late resolution, respectively). Liver H&E staining from females (A) and males (B) (green arrows, macrovesicular steatosis; yellow arrows, microvesicular steatosis; red arrows, hepatocyte ballooning degeneration; and blue arrows, inflammatory foci). Scores for steatosis (C), inflammation (D), and hepatocyte ballooning degeneration (E). Serum ALT activity (F). Data are expressed as mean ± SEM (n = 4 mice/group/gender). *$P < 0.05$ for control versus EtOH; ^$P < 0.05$ for peak ALD versus early or late resolution. Abbreviations: CV, central vein; PV, portal vein.
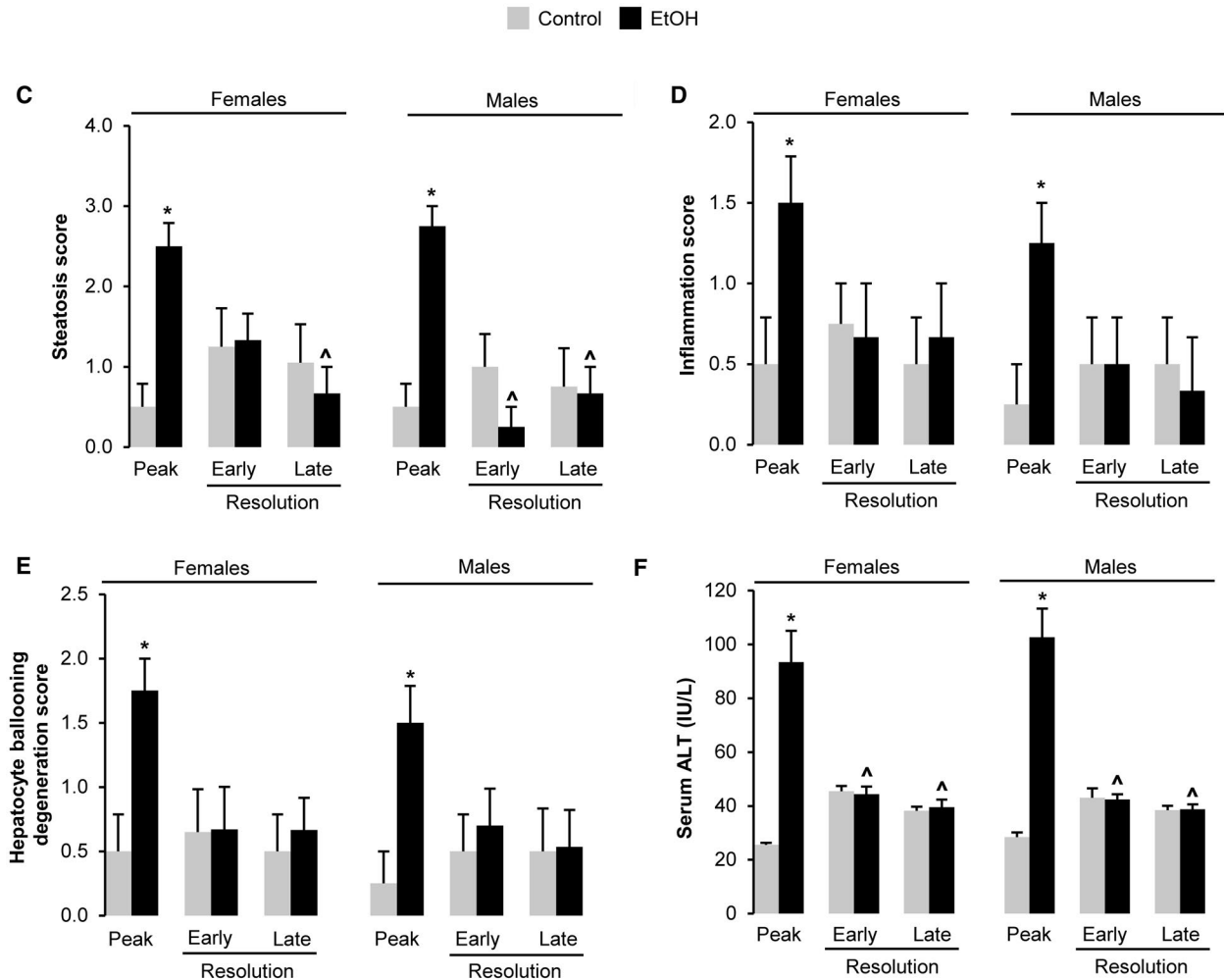
FIG. 1. Continued.

restored throughout resolution from ALD (Fig. 4A,B). Principal component analysis (PCA) revealed clear segregation among groups (Supporting Fig. S3A,B). Comparative analysis of the 55 genes with publicly available liver microarray data (GSE28619) from patients with alcohol-associated hepatitis (AH) (n = 15) and control livers (n = 3 cadaveric liver donors plus four resections of liver metastases) showed commonality with 40 genes linked to multiple pathways in males. PCA of the 40 common genes indicated clear segregation of patients with AH from controls in the microarray data set (Fig. 4C). There was comparative expression of the 40 genes in females at peak and resolution from ALD (Supporting Fig. S3C), and sparse partial least squares–discriminant analysis (PLS-DA) highlighted the 40 genes as discriminative features among groups (Supporting Fig. S3D). Furthermore,

using quantitative real-time PCR, the expression of the top 10 genes common among females, males, and human liver (GSE28619) was validated at peak and throughout resolution from ALD (Fig. 4D,E).

FECAL MICROBIOME AT PEAK AND RESOLUTION FROM ALD

Alcohol consumption alters the abundance and taxonomic composition of the intestinal microbiome, which contributes to progression of ALD.[11-13] Thus, we examined whether ceasing alcohol consumption could restore the intestinal microbiome and eventually facilitate disease resolution. To this end, fecal bacterial abundance and composition was analyzed. There were gender-specific changes in the abundance of total bacteria throughout ALD (Fig. 5A).
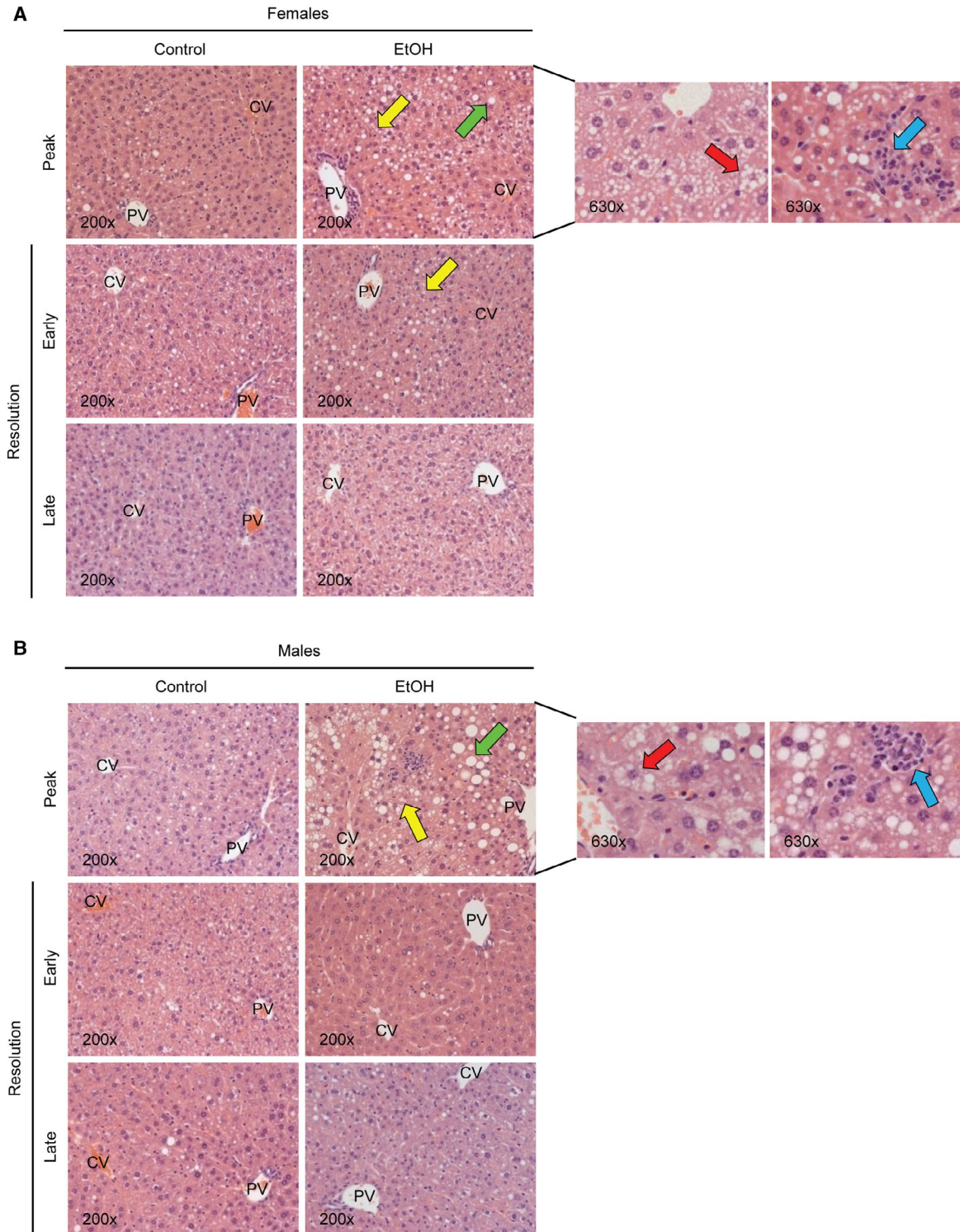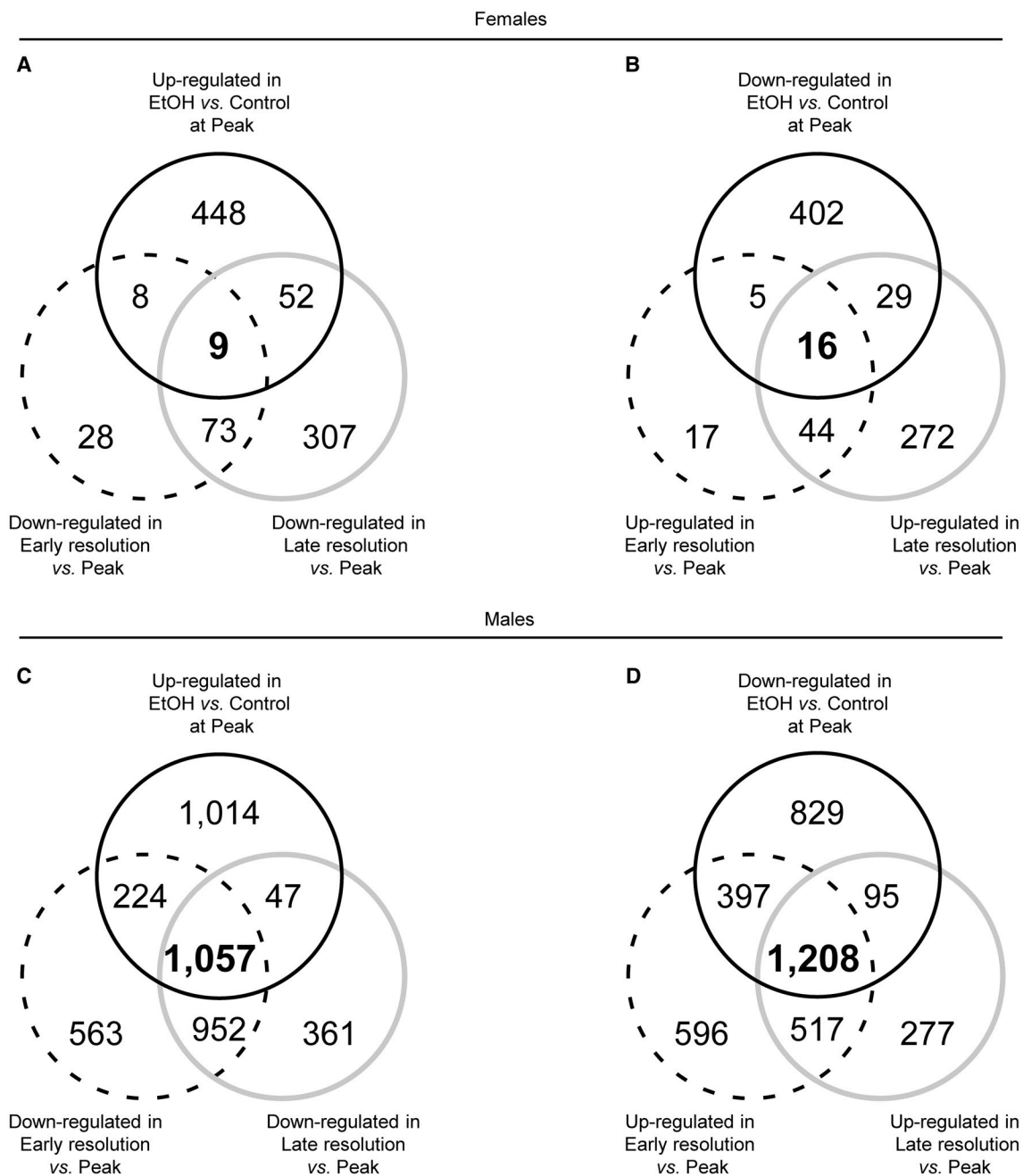
FIG. 2. Liver transcriptome at peak and resolution from ALD. Female and male WT mice were fed the control or ethanol LDC diets for 6 weeks (peak injury). To achieve resolution from ALD, mice were switched to control diet for 3 or 14 days (early or late resolution, respectively). Venn diagrams of dysregulated genes in females (A,B) and males (C,D) (n = 4 mice/group/gender). Genes with a FDR ≤ 0.05 were included in the analysis. For up-regulation a FC ≥ 1.5 and for down-regulation a FC ≤ 0.67 were considered.

There was no difference in microbial alpha diversity, suggesting microbial evenness at peak and resolution from ALD in both genders (Fig. 5B). Weighted UniFrac analysis showed clear separation of peak ALD from control-fed or ethanol-fed mice resolving from ALD (Fig. 5C,D). This suggests that the microbial composition at peak is qualitatively different from control-fed or ethanol-fed mice resolving from ALD. Seven bacterial fila were most abundant in both genders throughout ALD (Fig. 5E,F). The abundance of

these fila was markedly different between control-fed and ethanol-fed mice at peak and resolution from ALD (Supporting Fig. S4A,B). Several studies using other animal models of ALD or patients with alcoholism showed that alcohol affects these intestinal bacterial fila (Supporting Fig. S4C).

A Up-regulated (■) and down-regulated (▨) signaling pathways at peak and resolution from ALD in females
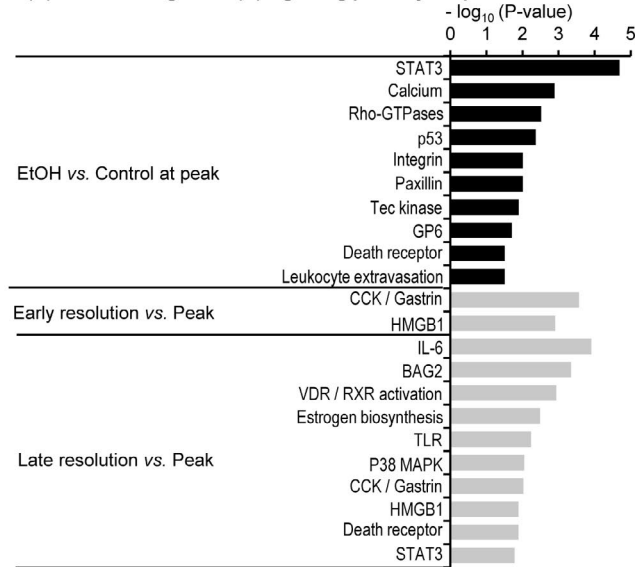
B Down-regulated (▨) and up-regulated (■) signaling pathways at peak and resolution from ALD in females
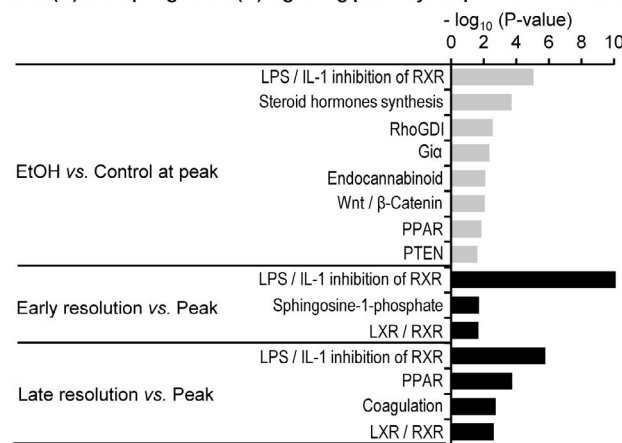
C Up-regulated (■) and down-regulated (▨) catabolic pathways at peak and resolution from ALD in females
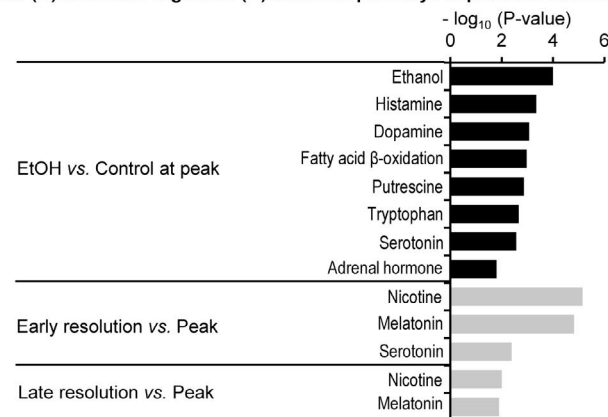
FIG. 3. Landscape of signaling pathways at peak and resolution from ALD. Female and male WT mice were fed the control or ethanol LDC diets for 6 weeks (peak injury). To achieve resolution from ALD, mice were switched to control diet for 3 or 14 days (early or late resolution, respectively). Pathway analysis in females: signaling (A,B) and catabolic (C) pathways. Pathway analysis in males: signaling (D,E), cellular stress and injury (F, top), and immune response (F, bottom) pathways (n = 4 mice/group/gender). Z-scores of pathways were considered for their activation status. Predicted activation (black) = positive Z-score and predicted inactivation (gray) = negative Z-score. Value of x-axis indicates the $-\log_{10} P$ value of the pathway. Abbreviations: APR, acute phase response; BAG2, Bcl2-associated athanogene 2; CCK, cholecystokinin; DC, dendritic cells; EGF, epidermal growth factor; FGF, fibroblast growth factors; Giα, Gi protein alpha subunit; Gp6, glycoprotein VI Platelet; HMGB1, high mobility group box 1 protein; Il-1, interleukin 1; Il-8, interleukin 8; IL-6, interleukin 6; JNK, Jun N-terminal kinase; LPS, lipopolysaccharides; LXR, liver X receptor; NF-κB, nuclear factor kappa light chain enhancer of activated B cells; NRF2, nuclear factor erythroid 2; OS, oxidative stress; P38 MAPK, p38 MAP Kinase; PPAR, peroxisome proliferator-activated receptor; PPARα, peroxisome proliferator-activated receptor alpha; PTEN, phosphatase and tensin homolog; ROS, reactive oxygen species; RNA, reactive nitrogen species; RXR, retinoid X receptor; RXRα, retinoid X receptor alpha; SPAK, STE20/SPS1-related proline alanine-rich kinase; TLR, toll-like receptor; TRK, tyrosine receptor kinase; VDR, vitamin D receptor.

Females at peak ALD showed higher abundance of two bacterial fila (Actinobacteria and Tenericutes) than control-fed mice (Fig. 6A). Actinobacteria decreased only in late resolution from ALD (Fig. 6A). Tenericutes decreased throughout resolution from ALD (Fig. 6A). Males at peak ALD showed more Deferribacteres than control-fed mice (Fig. 6B). Both Deferribacteres and Actinobacteria decreased throughout resolution from ALD (Fig. 6B).

Deeper analysis showed significant changes in abundance of a large number of bacterial genera at peak and resolution from ALD in females (Supporting Fig. S4D). Among these, *Corynebacterium1*, *Aerococcus*, *Ruminococcaceae UCG-014*, and *Alistipes* were more abundant at peak but decreased throughout resolution from ALD (Fig. 6C and Supporting Fig. S4D). In males, *Alistipes*, *RikenellaceaeRC9 gut group*, *Prevotellaceae UCG-001*, *Coriobacteriaceae UCG-002*, and *Rikenella* were more abundant at peak and decreased throughout resolution from ALD (Fig. 6D).

PORTAL SERUM METABOLOME AT PEAK AND RESOLUTION FROM ALD

The gut-liver axis plays a major role in ALD, as multiple metabolites, many of bacterial origin, translocate to the portal blood and enhance liver injury.[8] Disruption of the intestinal epithelial barrier, attributable to the effects of alcohol and its metabolites, increases gut permeability. As a result, pathogen-associated and damage-associated molecular patterns translocate from the gut lumen to the portal circulation and target the liver.[23] Therefore, we measured gut permeability i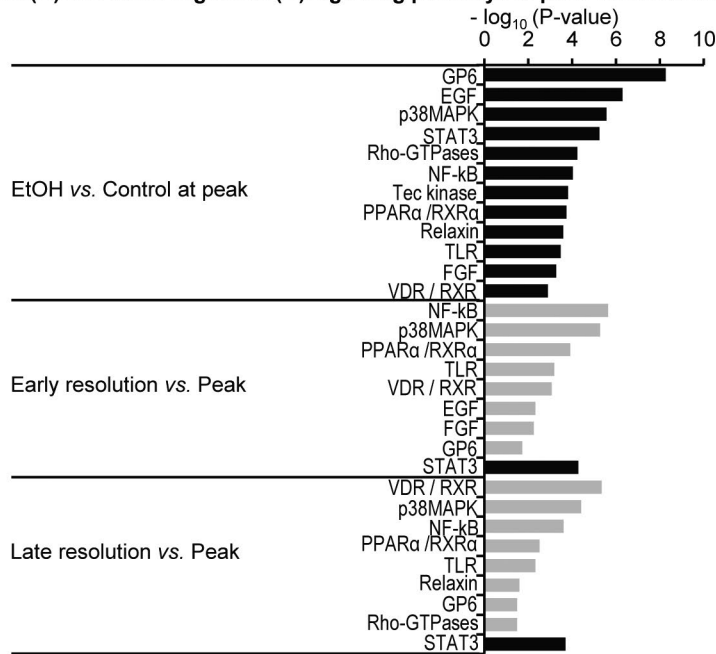n our model. In both genders, ethanol increased portal serum FITC-dextran but it returned to baseline during resolution from ALD (Supporting Fig. S5).

Next, we performed untargeted metabolomics in portal serum to identify metabolites translocated from the intestine to the portal serum, which could contribute to peak and resolution from ALD. We identified 281 metabolites in both genders at peak and resolution from ALD (data not shown). PCA and PLS-DA showed clear segregation and discrimination among groups (Supporting Fig. S6A-D). There were 10 top metabolites based on a variable's importance score of >1.8 in both genders (Supporting Fig. S6E,F). In females, tryptophan, tryptophan-NH$_3$, choline, glycyl-L-leucine, and xanthine were high, whereas 4-hydroxy-L-phenylglycine and N-acetylputrescine were low at peak; yet, in both cases, they reversed during early and/or late resolution from ALD (Fig. 6E). Males showed increased hexanesulfonic acid–sulfate, glycolate, glycyl-L-leucine and leucine-proline, and decreased urate at peak, and, except for the latter that continued decreasing, the others were restored throughout resolution from ALD (Fig. 6F).

PORTAL SERUM BAS AT PEAK AND RESOLUTION FROM ALD

Further analysis showed that several metabolites were 1.5-fold high or low at peak and resolution from ALD in both genders (Supporting Fig. S7A,B). Following identification of common metabolites at peak and resolution from ALD (FC ≥ 1.5), we performed pathway and metabolite enrichment analysis. These analyses revealed that most metabolites were associated with BA composition (Supporting Fig. S7C-F).

D   Up-regulated (■) and down-regulated (■) signaling pathways at peak and resolution from ALD in males

$-\log_{10}$ (P-value)

EtOH *vs.* Control at peak
- GP6
- EGF
- p38MAPK
- STAT3
- Rho-GTPases
- NF-kB
- Tec kinase
- PPARα /RXRα
- Relaxin
- TLR
- FGF
- VDR / RXR

Early resolution *vs.* Peak
- NF-kB
- p38MAPK
- PPARα /RXRα
- TLR
- VDR / RXR
- EGF
- FGF
- GP6
- STAT3

Late resolution *vs.* Peak
- VDR / RXR
- p38MAPK
- NF-kB
- PPARα /RXRα
- TLR
- Relaxin
- GP6
- Rho-GTPases
- STAT3

E   Down-regulated (■) and up-regulated (■) signaling pathways at peak and resolution from ALD in males

$-\log_{10}$ (P-value)

EtOH *vs.* Control at peak
- p53
- Neurotrophin / TRK
- Endocannabinoid
- SAPK / JNK
- Sphingosine-1-phosphate
- Micropinocytosis
- Rac
- LXR / RXR
- Thrombopoietin
- ErbB4
- Angiopoietin
- PPAR

Early resolution *vs.* Peak
- Sphingosine-1-phosphate
- LXR / RXR
- Micropinocytosis
- p53
- Thrombopoietin
- SAPK / JNK
- PPAR
- Neurotrophin / TRK
- Rac
- ErbB4
- Angiopoietin

Late resolution *vs.* Peak
- LXR / RXR
- Sphingosine-1-phosphate
- Micropinocytosis
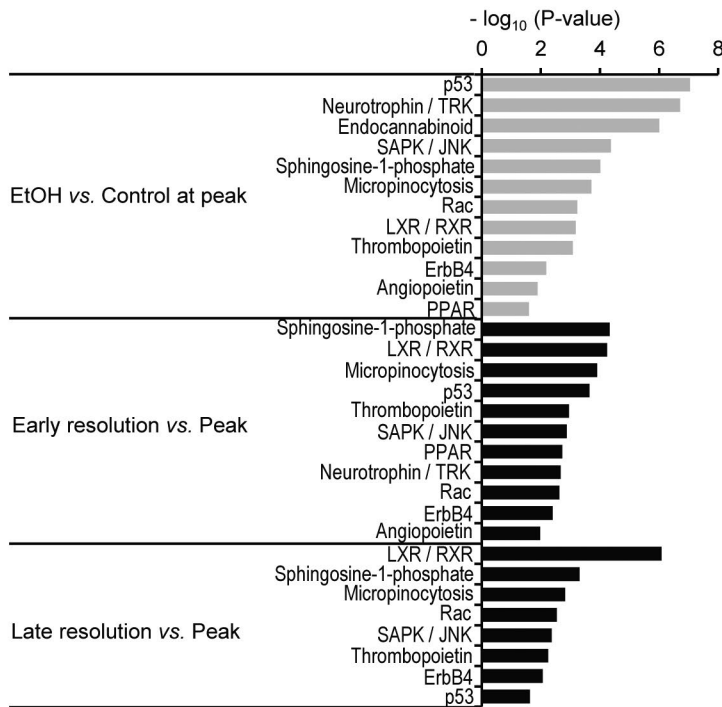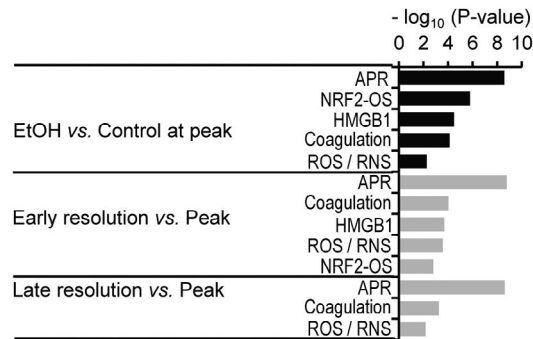- Rac
- SAPK / JNK
- Thrombopoietin
- ErbB4
- p53

FIG. 3. Continued.

F Up-regulated (■) and down-regulated (■) cellular stress and injury pathways at peak and resolution from ALD in males

$-\log_{10}$ (P-value)

Up-regulated (■) and down-regulated (■) cellular stress and injury pathways at peak and resolution from ALD in males
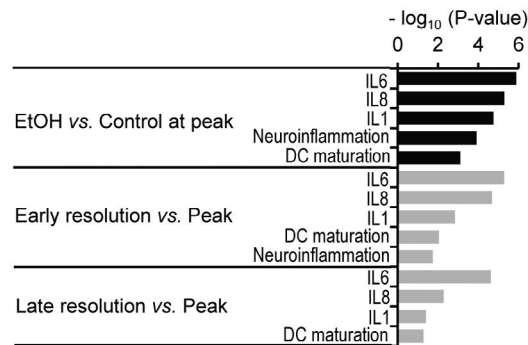
$-\log_{10}$ (P-value)

FIG. 3. Continued.

In females, cholic acid (CA), dimer of cholic acid (d-CA), dimer of deoxycholic acid, chenodeoxycholic acid (CDCA), and taurolithocholic acid (TLCA) increased, whereas taurocholic acid (TCA), taurodeoxycholic acid (TDCA), ursodeoxycholic acid (UDCA), and tauroursodeoxycholic acid decreased at peak ALD (Supporting Fig. S8A). In males, cholate, TCA, TDCA, and taurochenodesoxycholic acid (TCDCA) increased, whereas CA, d-CA, deoxycholic acid, CDCA, and UDCA decreased at peak ALD (Supporting Fig. S8A).

CORRELATION ANALYSIS OF BAS AND BACTERIAL FILA

Spearman's rank-correlation analysis showed that only a few BAs significantly correlated with the abundance of specific bacterial fila in a gender-specific manner (Supporting Fig. S8B). In females, CA, d-CA, and CDCA showed inverse correlation with Actinobacteria. LCA and TLCA showed direct correlation with Deferribacteres and/or Verrucomicrobia (Supporting Fig. S8B). In males, TCA and TCDCA showed direct correlation with Actinobacteria. Cholate and deoxycholate (DC) showed direct correlation, whereas CDCA and UDCA showed inverse correlation with Deferribacteres (Supporting Fig. S8B). Overall, these findings suggest that alcohol alters intestinal BA composition in a gender-specific manner, and intestinal dysbiosis may contribute to it.

## INTEGRATION AMONG THE GUT MICROBIOME, PORTAL SERUM METABOLOME, AND LIVER TRANSCRIPTOME

To investigate the relationship between the gut microbiome and portal serum metabolome as well as their potential role in peak and resolution from ALD, we performed Spearman's rank correlation between bacterial genera and metabolites (Fig. 7A,B). In females, *Corynebacterium1*, *Aerococcus*, and *Ruminococcaceae*

143

UCG-014 showed significant direct correlation with choline and glycyl-L-leucine, but inverse correlation with hydroxy-L-phenylglycine and N-acetylputrescine (Fig. 7A). In males, *Alistipes*, *RikenellaceaeRC9 gut* *group*, *Prevotellaceae UCG-001*, *Coriobacteriaceae UCG-002*, and *Rikenella* showed positive correlation with hexanesulfonic acid–sulfate, glycolate, glycyl-L-leucine, and leucine-proline in portal sera (Fig. 7A).

A **Heatmap of genes linked to multiple altered pathways in females**
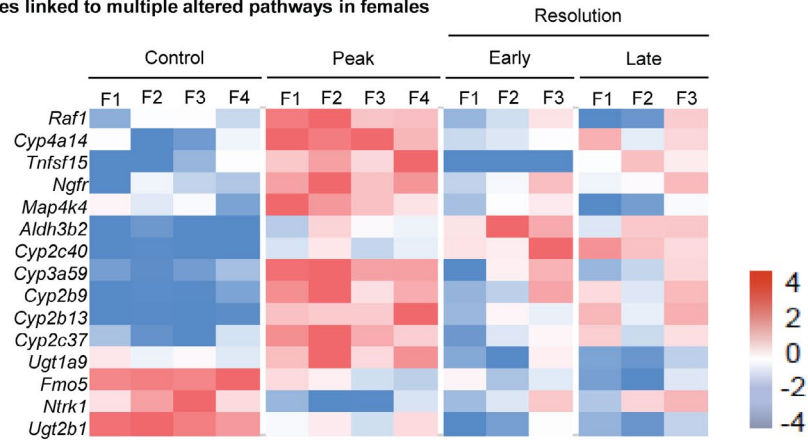
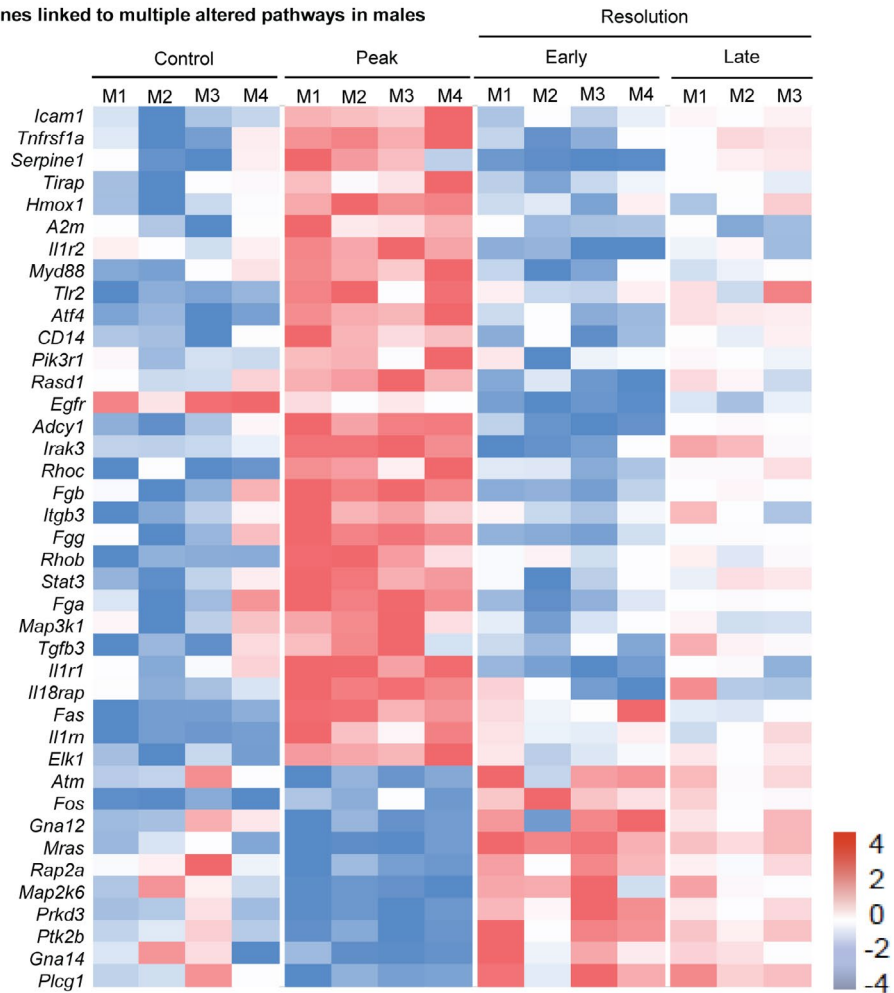**B** **Heatmap of genes linked to multiple altered pathways in males**

FIG. 4. Common genes in pathways changed at peak and restored throughout resolution from ALD. Female and male WT mice were fed the control or ethanol LDC diets for 6 weeks (peak injury). To achieve resolution from ALD, mice were switched to control diet for 3 or 14 days (early or late resolution, respectively). Heatmap of genes linked to multiple pathways altered at peak and resolution from ALD in females (A) and males (B) (n = 4 mice/group/gender). PCA of common genes found in the publicly available liver microarray data set (GSE28619) (C). Relative expression of the top 10 genes at peak and resolution from ALD in females (D) and males (E). Data are expressed as mean ± SEM (n = 4 mice/group/gender). *P < 0.05 and **P < 0.01 for control versus peak; $^\wedge P$ < 0.05 and $^{\wedge\wedge}P$ < 0.01 for peak ALD versus early or late resolution. Abbreviations: *A2m*, alpha-2-macroglobulin; *Adcy1*, adenylate cyclase 1; *Aldh3b2*, aldehyde dehydrogenase 3 family member B2; *Atf4*, activating transcription factor 4; *Atm*, ataxia telangiectasia mutated; *Cd14*, monocyte differentiation antigen Cd14; *Cyp2b9*, cytochrome P450, family 2, subfamily b, polypeptide 9; *Cyp2b13*, cytochrome P450, family 2, subfamily b, polypeptide 13; *Cyp2c37*, cytochrome P450, family 2, subfamily c, polypeptide 37; *Cyp2c40*, cytochrome P450, family 2, subfamily c, polypeptide 40; *Cyp3a59*, cytochrome P450, family 3, subfamily a, polypeptide 59; *Cyp4a14*, cytochrome P450, family 4, subfamily a, polypeptide 14; *Egfr*, epidermal growth factor receptor; *Elk1*, ELK1, member of ETS oncogene family; *Fga*, fibrinogen alpha chain; *Fgb*, fibrinogen beta chain; *Fgg*, fibrinogen gamma chain; *Fas*, Fas (TNF receptor superfamily member 6); *Fmo5*, flavin containing monooxygenase 5; *Fos*, FBJ osteosarcoma oncogene; *Gna12*, G protein subunit alpha 12; *Gna14*, G protein subunit alpha 14; *Hmox1*, heme oxygenase 1; *Icam1*, intercellular adhesion molecule 1; *Il1r1*, interleukin 1 receptor, type I; *Il1r2*, interleukin 1 receptor, type II; *Il18rap*, interleukin 18 receptor accessory protein; *Il1rn*, interleukin 1 receptor antagonist; *Irak3*, interleukin-1 receptor-associated kinase 3; *Itgb3*, integrin beta 3; *Map3k1*, mitogen-activated protein kinase kinase kinase 1; *Map4k4*, mitogen-activated protein kinase kinase kinase kinase 4; *Mras*, muscle and microspikes RAS; *Map2k6*, mitogen-activated protein kinase kinase 6; *Myd88*, myeloid differentiation primary response gene 88; *Ngfr*, nerve growth factor receptor; *Ntrk1*, neurotrophic tyrosine kinase, receptor, type 1; PC, principal component; *Pik3r1*, phosphatidylinositol 3-kinase regulatory subunit alpha; *Plcg1*, phospholipase C, gamma 1; *Prkd3*, protein kinase D3; *Ptk2b*, PTK2 protein tyrosine kinase 2 beta; qRT-PCR, quantitative real-time PCR; *Raf1*, v-raf-leukemia viral oncogene 1; *Rap2a*, RAS related protein 2a; *Rasd1*, RAS, dexamethasone-induced 1; *Rhob*, ras homolog family member B; *Rhoc*, ras homolog family member C; *Serpine1*, serine (or cysteine) peptidase inhibitor, clade E, member 1; *Stat3*, signal transducer and activator of transcription 3; *Tgfb3*, transforming growth factor beta 3; Tirap, toll-interleukin 1 receptor (TIR) domain-containing adaptor protein; *Tlr2*, toll-like receptor 2; *Tnfrsf1a*, tumor necrosis factor receptor superfamily, member 1a; *Tnfsf15*, tumor necrosis factor (ligand) superfamily, member 15; *Ugt1a9*, UDP glucuronosyltransferase 1 family, polypeptide A9; *Ugt2b1*, UDP glucuronosyltransferase 2 family, polypeptide b1.

Moreover, the changes in bacterial genera or metabolites showed significant correlation with some of the altered genes and in a gender-specific manner (Fig. 7B). In males, the number of significantly correlating genes and bacterial genera was high (Fig. 7B). In both genders, *Map3k1*, *Stat3*, activating transcription factor 4 (*Atf4*), serpin family E member 1 (*Serpine1*), *Tlr2*, *Cd14*, heme oxygenase 1 (*Hmox1*), and Ras homolog gene family, member C (*Rhoc*) significantly correlated with a greater number of bacterial genera and portal serum metabolites (Fig. 7B). Analysis of the expression of these eight genes in publicly available human liver microarray data sets (GSE28619 and GSE14 3318) indicated significantly high expression of *MAP3K1* in patients with AH compared to healthy controls (HC) (Fig. 7C). Moreover, in both genders, *Map3k1* increased at peak and declined throughout resolution from ALD (Fig. 4D,E).

Validation by IHC and WB revealed high expression of MAP3K1 in liver sections and lysate at peak and reduction throughout resolution from ALD, which occurred in both genders (Fig. 7D,E). Ethanol-fed mice displayed enhanced nuclear localization of MAP3K1 that declined throughout resolution from ALD (Fig. 7D).

In addition, we analyzed the expression of MAP3K1 in liver from patients with AH (n = 3) and HC (n = 3). MAP3K1 increased by 2-fold in livers from patients with AH compared to HC (Fig. 7F). Overall, these findings suggest that alcohol consumption, directly and/or indirectly through the gut-liver axis, induces the hepatic expression of *MAP3K1*, which participates in the pathogenesis and resolution from ALD.

INHIBITION OF MAP3K1 PROTECTS FROM ALD

To investigate the link between MAP3K1 and ALD, we administered mice PEITC, an inhibitor of MAP3K1 activity, during progression and resolution from ALD. WB analysis showed reduced phosphorylation of JNK, a MAP3K1 downstream target, in PEITC-treated mice, confirming inhibition of MAP3K1 activity (Fig. 8A).

Although there was increased steatosis, hepatocyte ballooning degeneration, and inflammation, ALT and AST activates liver TGs and CHO in ethanol-fed mice at peak compared with controls. Importantly, inhibition of MAP3K1 with PEITC reduced all of these

C **PCA scores plot of genes linked with multiple altered pathways in dataset GSE28619**
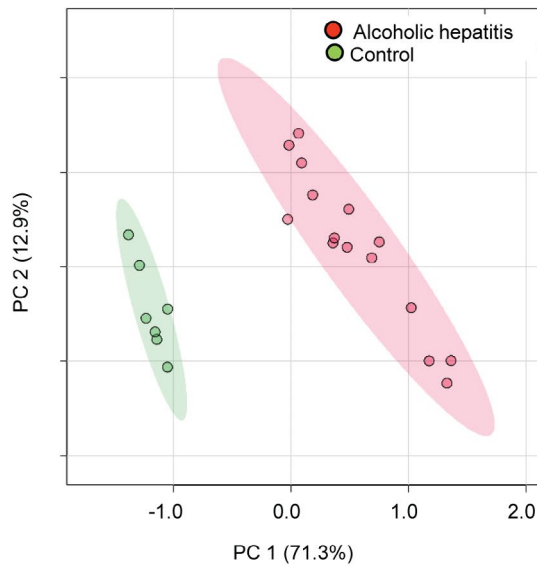
D **qRT-PCR validation in females**
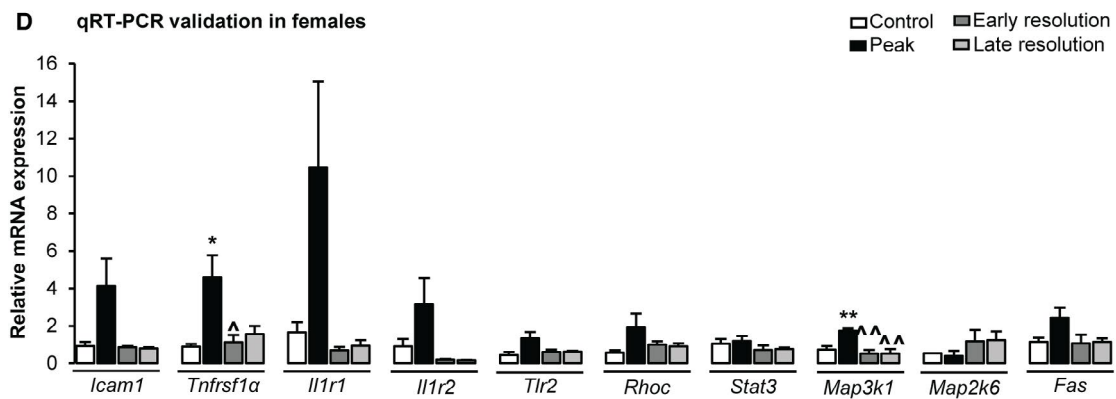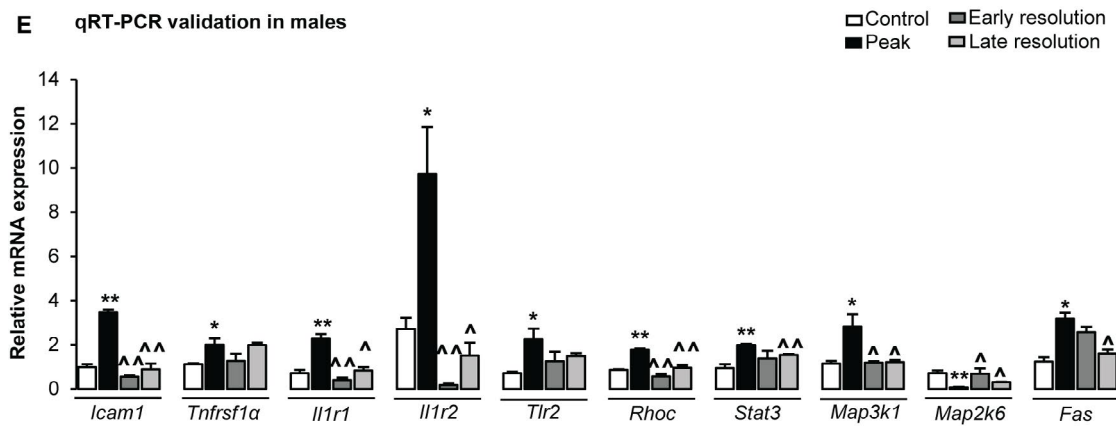

E **qRT-PCR validation in males**

FIG. 4. Continued.

FIG. 5. Fecal microbiome at peak and resolution from ALD. Female and male WT mice were fed the control or ethanol LDC diets for 6 weeks (peak injury). To achieve resolution from ALD, mice were switched to control diet for 3 or 14 days (early or late resolution, respectively). Abundance of total bacteria in feces (A). Alpha diversity in intestinal bacteria based on the Shannon Index (B). PCA plot of weighted UniFrac distances in females (C) and males (D). Operational taxonomic units (%) of identified bacterial fila in females (E) and males (F). Data are expressed as mean ± SEM (n = 4 mice/group/gender). Abbreviations: OTU, operational taxonomic unit; PC, principal component.

parameters (Fig. 8B,C and Supporting Fig. S9A,B). At peak ALD, all mice showed similar concentration of ethanol in serum, suggesting that PEITC does not alter ethanol metabolism (Supporting Fig. S9A,B).

IHC analysis showed increased cytosolic staining and nuclear localization of MAP3K1 in ethanol-fed mice at peak ALD (Fig. 8D). To identify what triggers

MAP3K1 nuclear localization, primary hepatocytes were treated with a polyunsaturated fatty acid (arachidonic acid [AA]), ethanol, AA plus ethanol, LPS, TNFα, IL-1β, and H_2O_2, all known to be involved in ALD. WB analysis revealed increased MAP3K1 expression in the cytosol and nucleus only in hepatocytes treated with ethanol alone or with AA (Fig. 8E).

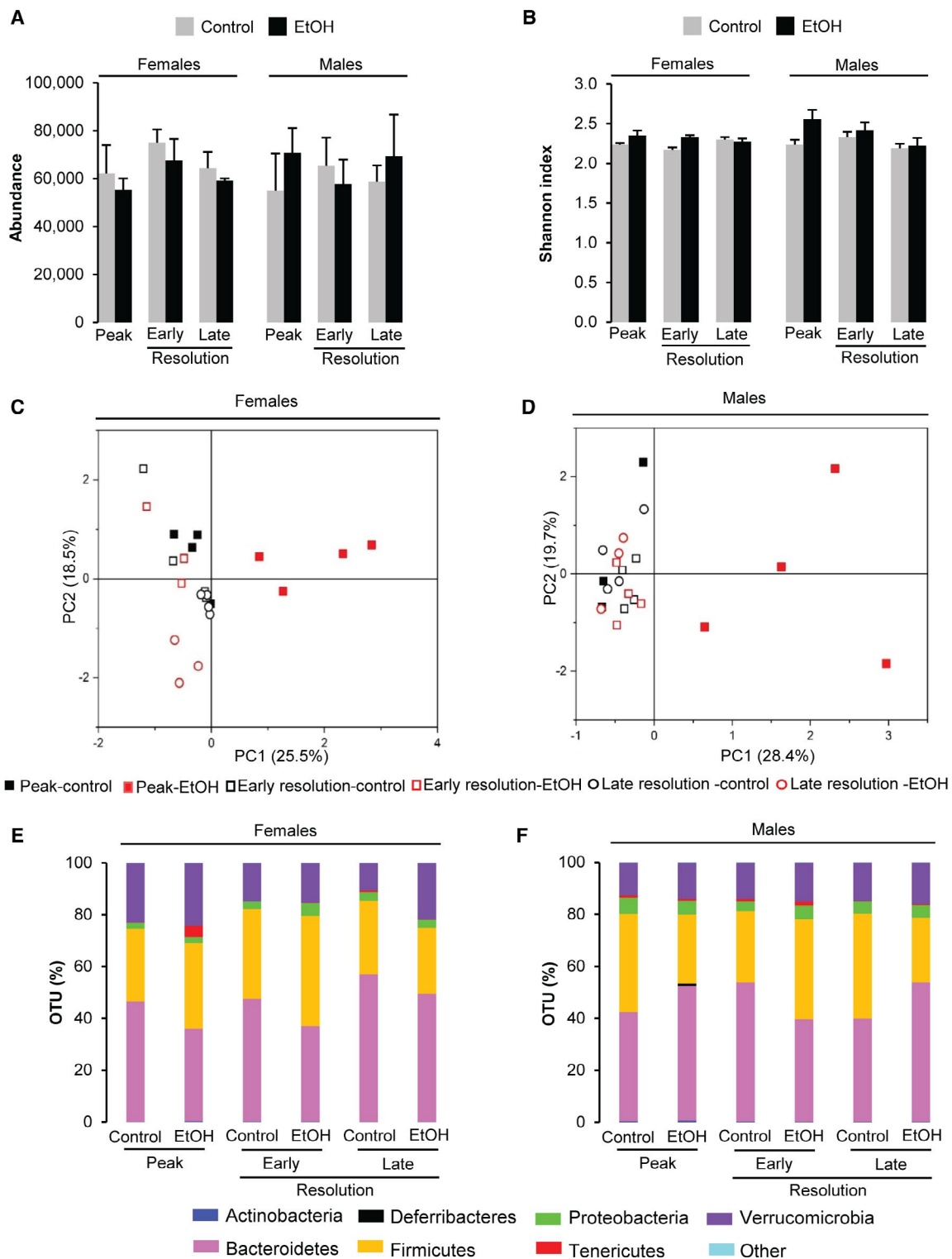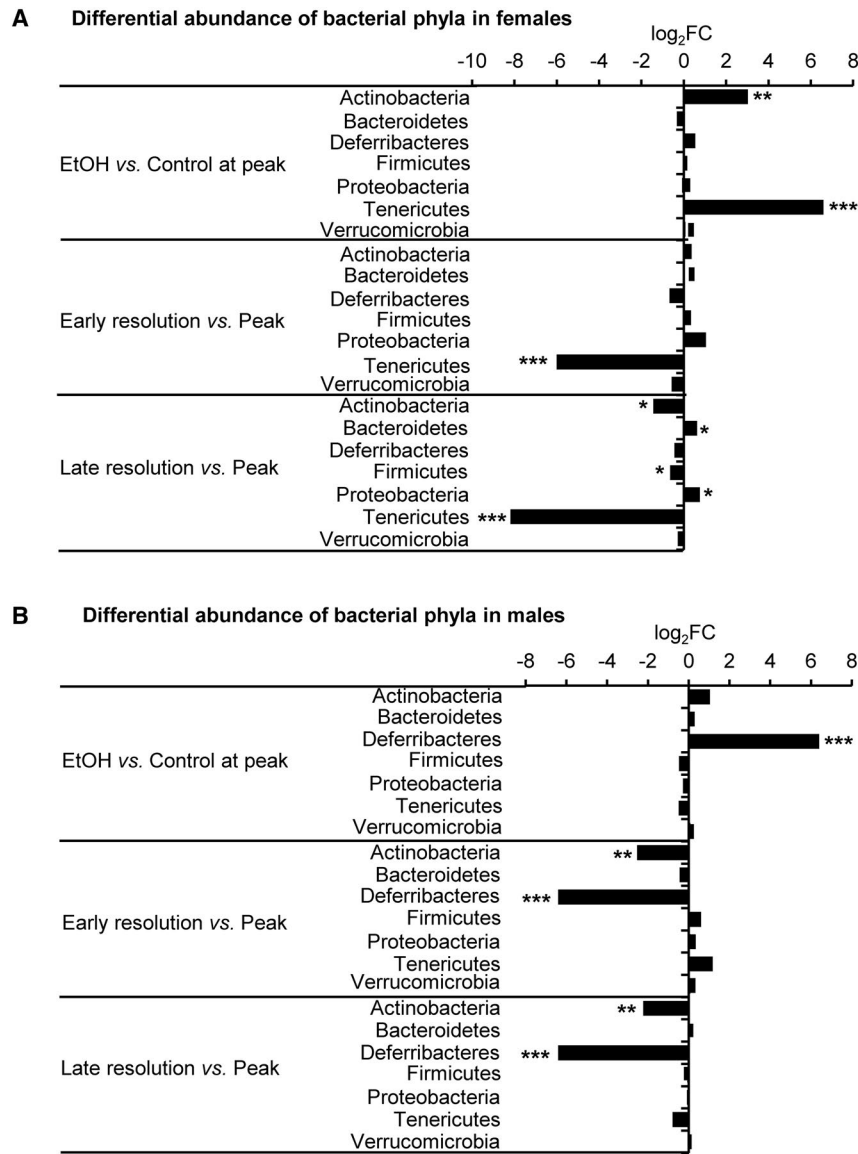**FIG. 6.** Changes in the microbiome and portal serum metabolome at peak and resolution from ALD. Female and male WT mice were fed the control or ethanol LDC diets for 6 weeks (peak injury). To achieve resolution from ALD, mice were switched to control diet for 3 or 14 days (early or late resolution, respectively). Differential analysis of bacterial fila in females (A) and males (B). Differential analysis of bacterial genera in females (C) and males (D). Differential analysis of portal serum metabolites in females (E) and males (F). The Venn diagrams (top) show the number of significantly altered bacterial genera or metabolites. The bar diagrams (bottom) show changes in abundance of bacterial genera or metabolites at peak and throughout resolution from ALD. Log$_2$ FC = fold change in abundance of bacterial taxa or metabolites, + increase and − decrease in abundance (n = 4 mice/group/gender). *FDR < 0.05, **FDR < 0.01, and ***FDR < 0.001.

The hepatic mRNA expression of genes involved in lipogenesis (sterol regulatory element binding transcription factor 1 [*Srebp1*], fatty acid synthase [*Fasn*], acetyl-CoA carboxylase 1 [*Acaca*], ATP citrate synthase [*Acly*], and *Pparg*) and inflammation (*Tnfa*, *Il-1r1*, and *Il-1r2*) increased in ethanol-fed mice at peak
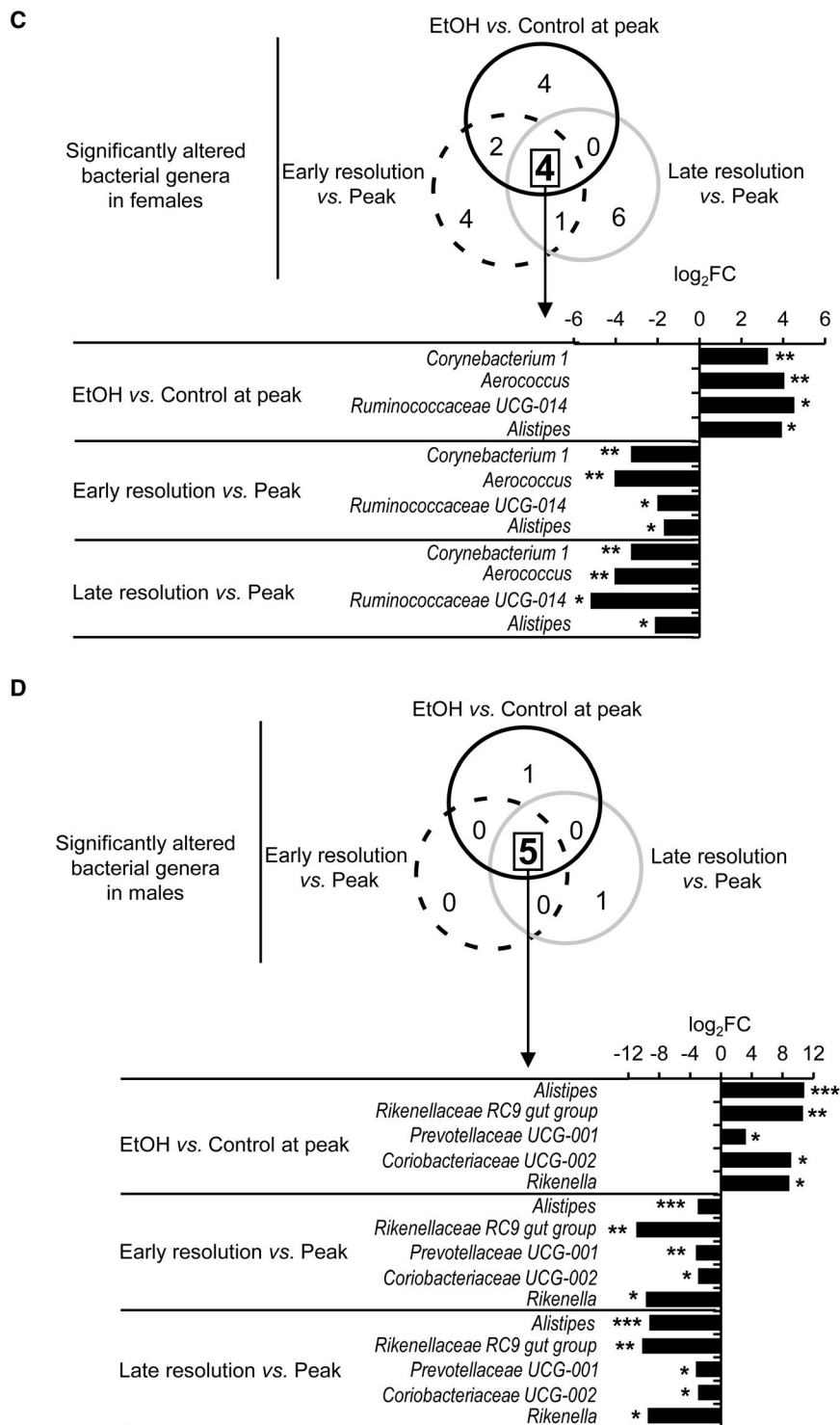
FIG. 6. Continued.
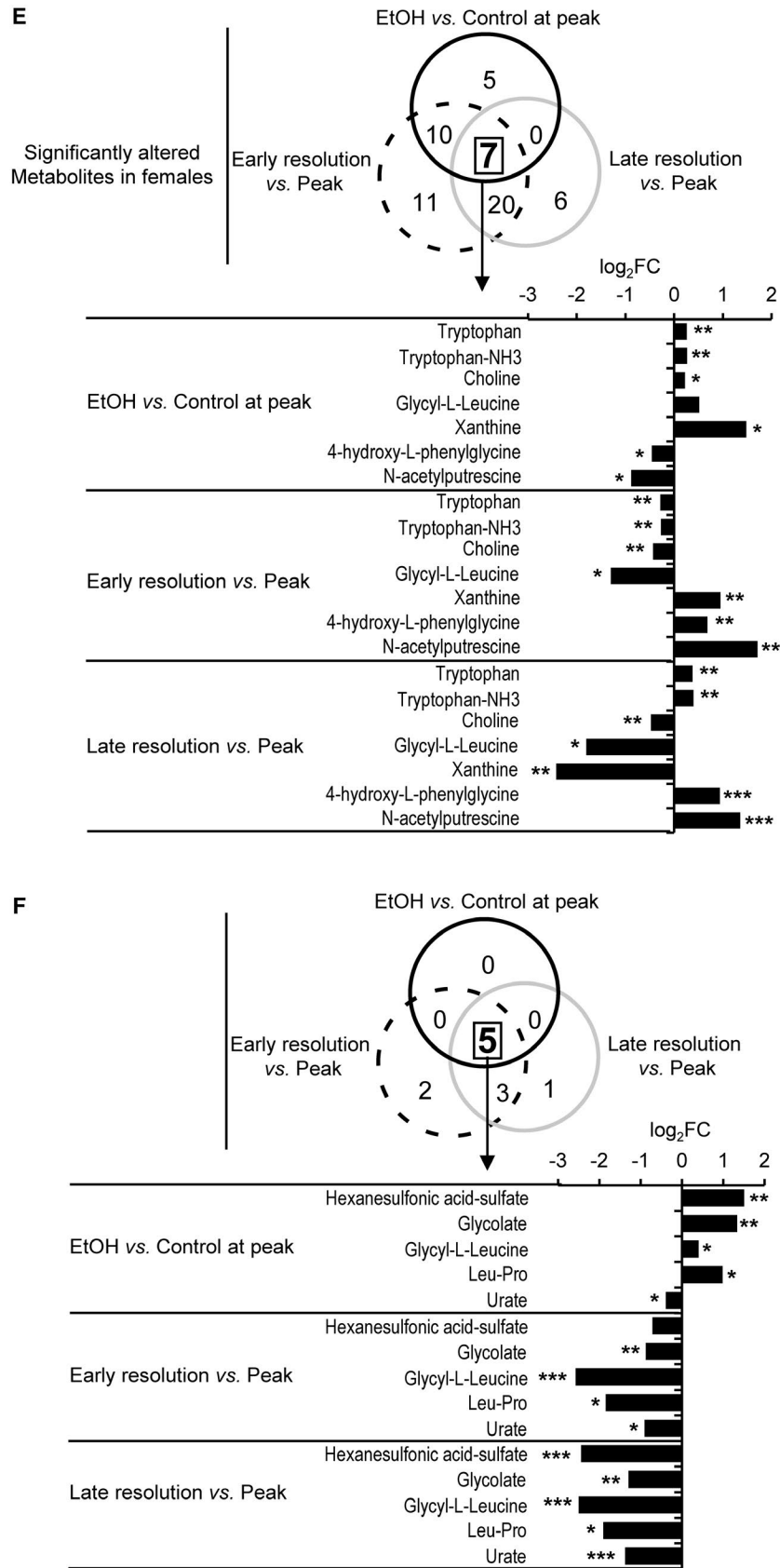
FIG. 6. Continued.

ALD; however, co-treatment with PEITC reduced them (Fig. 8F top and middle). Finally, we isolated primary hepatocytes and co-treated them with ethanol in the presence or absence of PEITC. Quantitative real-time PCR analysis also showed down-regulation in the lipogenic and pro-inflammatory genes (Fig. 8F bottom). In summary, these results suggest that MAP3K1 contributes to pathogenesis in ALD.

Discussion

In the present study, we unveil the gender-specific liver transcriptome, fecal microbiome, and portal serum metabolome at peak injury and resolution from ALD. We integrate their interactions to obtain the "multiomics" landscape and understand better the pathogenesis of ALD.

FIG. 7. Integration among the gut microbiome, portal serum metabolome, and liver transcriptome. Female and male WT mice were fed the control or ethanol LDC diets for 6 weeks (peak injury). To achieve resolution from ALD mice were switched to control diet for 3 or 14 days (early or late resolution, respectively). Spearman's rank correlation plot depicting the correlation be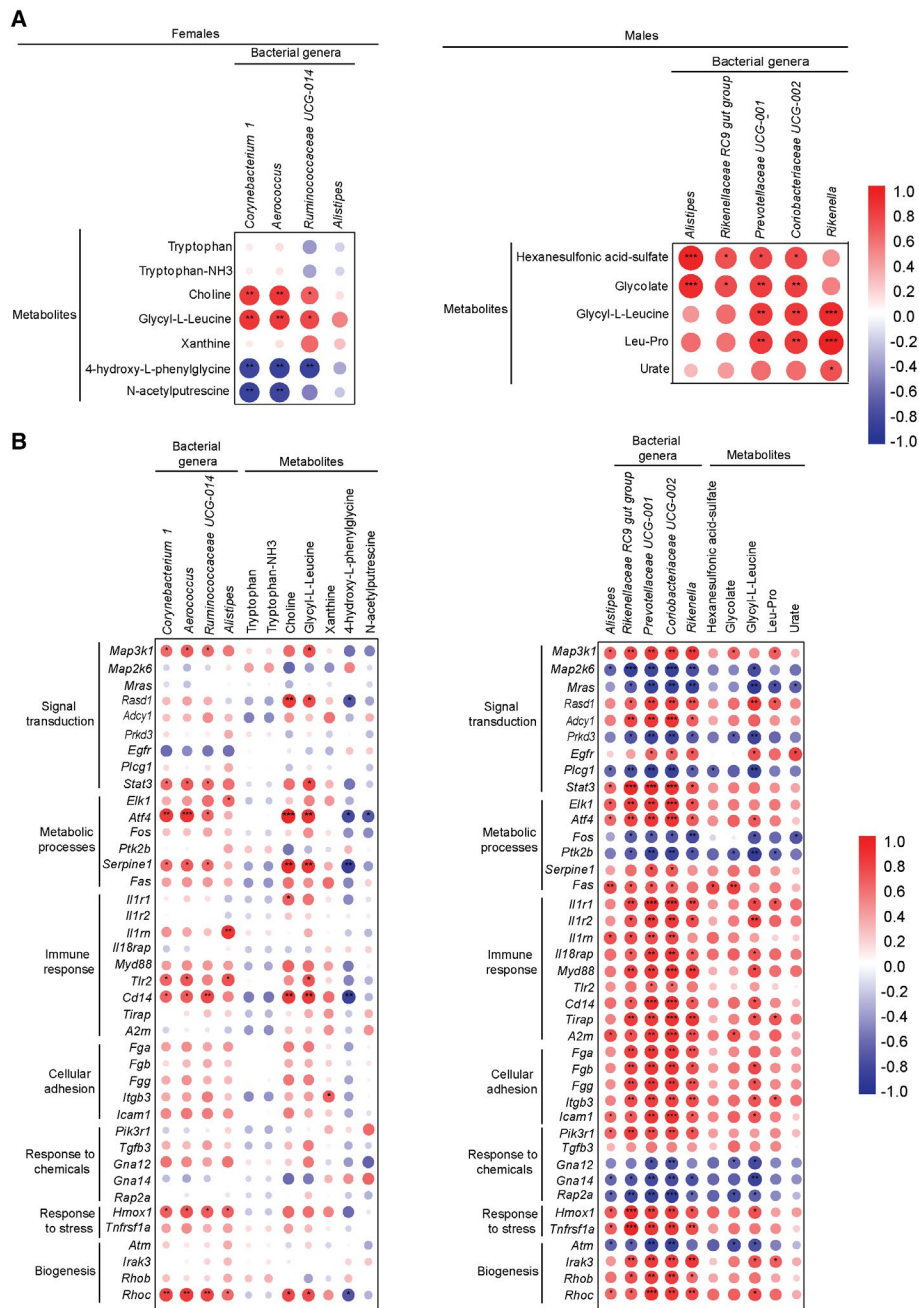tween metabolites and bacteria in females and males (A). Spearman's rank correlation plot depicting the correlation between genes and bacteria or metabolites in females and males. Color intensity and circle size represent the magnitude of the correlation. Asterisks indicate the significance of the correlation ($*P < 0.05$, $**P < 0.01$, and $***P < 0.001$) (B). *MAP3K1* mRNA expression in publicly available liver microarray data sets (GSE28619: n = 15 patients with AH and n = 7 HC [n = 3 cadaveric liver donors plus four resections of liver metastases]; GSE143318: n = 5 patients with severe AH and 5 HC) (C). IHC for MAP3K1 in liver sections from females and males (orange arrow = MAP3K1-positive nucleus in hepatocytes) (D). Western blot of MAP3K1 in livers from females and males (n = 3 mice/group/gender) (E) and in patients with AH (n = 3) and HC (n = 3) (F) normalized to Calnexin. Data are expressed as mean ± SEM. $**P < 0.01$ for control versus alcohol; $^{\wedge}P < 0.05$ and $^{\wedge\wedge}P < 0.01$ for peak ALD versus early or late resolution; $^{\#\#}P < 0.01$ and $^{\#\#\#}P < 0.001$ for patients with AH or severe AH (SAH) versus HC or control. Abbreviation: *A2m*, alpha-2-macroglobulin; *Adcy1*, adenylate cyclase 1; *Atf4*, activating transcription factor 4; *Atm*, ataxia telangiectasia mutated; *Cd14*, monocyte differentiation antigen Cd14; *CV*, central vein; *Egfr*, epidermal growth factor receptor; *Fga*, fibrinogen alpha chain; *Fgb*, fibrinogen beta chain; *Fgg*, fibrinogen gamma chain; *Elk1*, ELK1, member of ETS oncogene family; *Fas*, Fas (TNF receptor superfamily member 6); *Fos*, FBJ osteosarcoma oncogene; *Gna12*, G protein subunit alpha 12; *Gna14*, G protein subunit alpha 14; *Hmox1*, heme oxygenase 1; *Icam1*, intercellular adhesion molecule 1; *Il1r1*, interleukin 1 receptor, type I; *Il1r2*, interleukin 1 receptor, type II; *Il18rap*, interleukin 18 receptor accessory protein; *Il1rn*, interleukin 1 receptor antagonist; *Irak3*, interleukin-1 receptor-associated kinase 3; *Itgb3*, integrin beta 3; *Map3k1*, mitogen-activated protein kinase kinase kinase 1; *Mras*, muscle and microspikes RAS; *Map2k6*, mitogen-activated protein kinase kinase 6; *Myd88*, myeloid differentiation primary response gene 88; *Pik3r1*, phosphatidylinositol 3-kinase regulatory subunit alpha; *Plcg1*, phospholipase C, gamma 1; *Prkd3*, protein kinase D3; *Ptk2b*, PTK2 protein tyrosine kinase 2 beta; *Rap2a*, RAS related protein 2a; *Rasd1*, RAS, dexamethasone-induced 1; *Rhob*, ras homolog family member B; *Rhoc*, ras homolog family member C; *Serpine1*, serine (or cysteine) peptidase inhibitor, clade E, member 1; *Stat3*, signal transducer and activator of transcription 3; *Tgfb3*, transforming growth factor beta 3; *Tirap*, toll-interleukin 1 receptor (TIR) domain-containing adaptor protein; *Tlr2*, toll-like receptor 2; *Tnfrsf1a*, tumor necrosis factor receptor superfamily, member 1a.

We reveal that a significant number of genes up-regulated or down-regulated during peak are restored during resolution from ALD. Thus, key signaling pathways return to baseline levels and likely facilitate the recovery from ALD. These changes are gender-specific and are more pronounced in males. Further studies are needed to clarify whether the limited number of genes altered in females result from the effect of estrogens, known to protect against progression of chronic liver disease.[24,25]

In females, only a few pathways (STAT3, death receptor, LPS/IL-1-mediated inhibition of RXR function, PPAR and serotonin degradation) are restored throughout resolution from ALD. In contrast, in males, almost all signaling pathways identified (Gp6, p38 MAPK, nuclear factor kappa B [NF-κB], PPARα/RXRα, TLR, vitamin D receptor/RXR, p53, stress-activated protein kinase [SAPK]/JNK, sphingosine-1-phosphate, micropinocytosis, Rac, liver X receptor/RXR, thrombopoietin, and ErbB4) return to baseline. Of note, STAT3 signaling remains activated throughout resolution from ALD in males but not in females; thus, it could be a tipping point responsible for the gender differences in ALD. In addition, males appear to achieve a more complete recovery from alcohol-induced liver injury and steatosis by day 3, compared with females, suggesting that the rate of recovery from ALD was not identical in both genders.

Signal transduction through the identified pathways plays a key role in onset and progression of ALD.[4,7,26-29] Restoration of these pathways due to alcohol withdrawal, as observed in this study, suggests that ethanol might directly target them, and inhibition of RXR can be a common pathway to protect from ALD in both genders (although this needs further validation). Indeed, in $Rxr^{-/-}$ mice, the activity of the ethanol-metabolizing cytochrome P450 2E1 is reduced[30] and is not induced by ethanol.[31] Therefore, inhibition or activation of these signals could be therapeutic to resolve ALD.

Changes in the fecal microbiota also contribute to ALD progression.[12,13] We show that ethanol has gender-specific effects on the abundance and composition of the fecal microbiome at peak and resolution from ALD. Particularly in females, ethanol strongly affects the Tenericutes filum, whereas, in males, it strongly affects the Deferribacteres filum. Both are gram-negative bacteria and a source of LPS; thus, if translocated, they will enhance alcohol-induced liver injury. Because ethanol administration causes overgrowth of these fila, and ethanol withdrawal reduces them, it is likely that targeting these phyla in a gender-specific manner could help to ameliorate ALD. This needs further functional validation.

Additionally, we demonstrate commonality in intestinal dysbiosis between females and males.

C

GSE28619 (microarray)

GSE143318 (microarray)

D
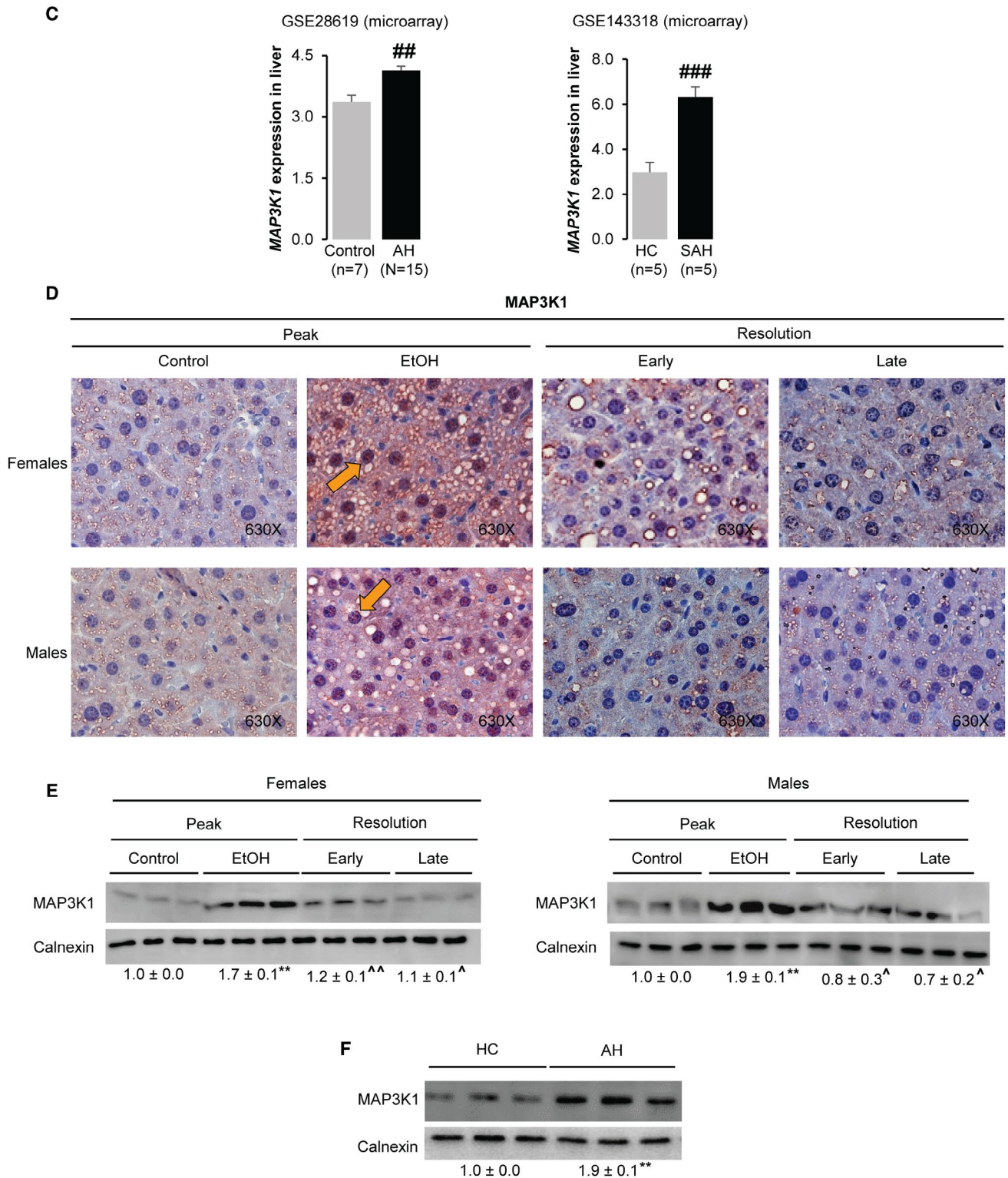
MAP3K1

E

F

FIG. 7. Continued.

Particularly in the case of the *Alistipes* genus, both genders show significant overgrowth during peak, which declines throughout resolution from ALD, suggesting that the effect of alcohol in this genus is not gender-restricted. *Alistipes* is a relatively new genus of bacteria under the filum Bacteroidetes, is

present in humans,[32] and is associated with intestinal inflammation[32]; therefore, alcohol-induced overgrowth of *Alistipes* could lead to intestinal inflammation in ALD.[33]

The data also reveal that alcohol changes intestinal metabolites, as shown by others,[14] but return to baseline values after abstinence. The significantly altered metabolites in portal serum at peak injury, restored throughout resolution from ALD, differ in females and males, suggesting that alcohol affects intestinal metabolism in a gender-specific manner. Nonetheless, glycyl-L-leucine increases at peak and declines throughout resolution from ALD in both genders. This dipeptide is typically produced as a result of incomplete breakdown of proteins; therefore, alcohol likely increases intestinal protein catabolism.
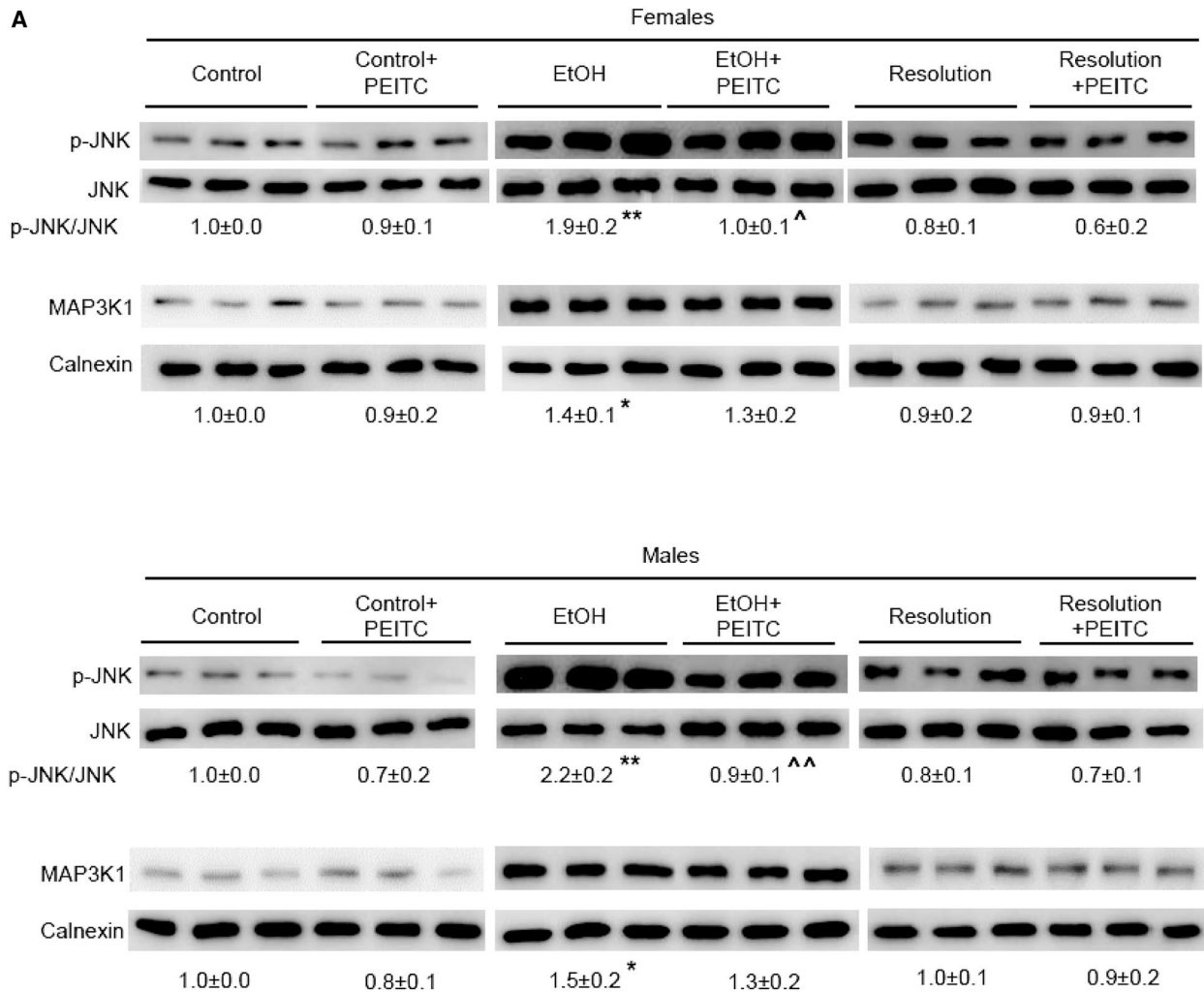

FIG. 8. Inhibition of MAP3K1 protects from ALD. Female and male WT mice were fed the control or ethanol LDC diets with or without PEITC for 6 weeks (peak injury). To achieve early resolution from ALD, mice were switched to control diet with or without PEITC for 3 days. Western blot of p-JNK, total JNK, and MAP3K1 in livers from females and males (n = 3 mice/group/gender) (A). Liver H&E staining from females and males (green arrows, macrovesicular steatosis; yellow arrows, microvesicular steatosis; red arrows, hepatocyte ballooning degeneration; and blue arrows, inflammatory foci) (B). Scores for steatosis, inflammation, hepatocyte ballooning degeneration, and serum ALT activity (C). IHC for MAP3K1 in livers from female and male mice (orange arrows, MAP3K1-positive nuclear staining in hepatocytes) (D). Western blot of MAP3K1 in the nuclear (E, left) and cytosolic fractions (E, right) from primary hepatocytes treated with AA, EtOH, or both (n = 3/treatment). Relative expression of lipogenic and pro-inflammatory genes in livers from female and male mice at peak and resolution from ALD with and without PEITC (F, top and middle, respectively) and in primary hepatocytes (F, bottom). Data are expressed as mean ± SEM (n = 4 mice/group/gender or n = 3 hepatocyte replicates/treatment). *$P < 0.05$, **$P < 0.01$, and ***$P < 0.001$ for control versus EtOH; ^$P < 0.05$ and ^^$P < 0.01$ for EtOH versus EtOH + PEITC; and ttt$P < 0.001$ for control versus EtOH or EtOH + AA. Abbreviations: CV, central vein; GAPDH, glyceraldehyde 3-phosphate dehydrogenase; PV, portal vein.

B
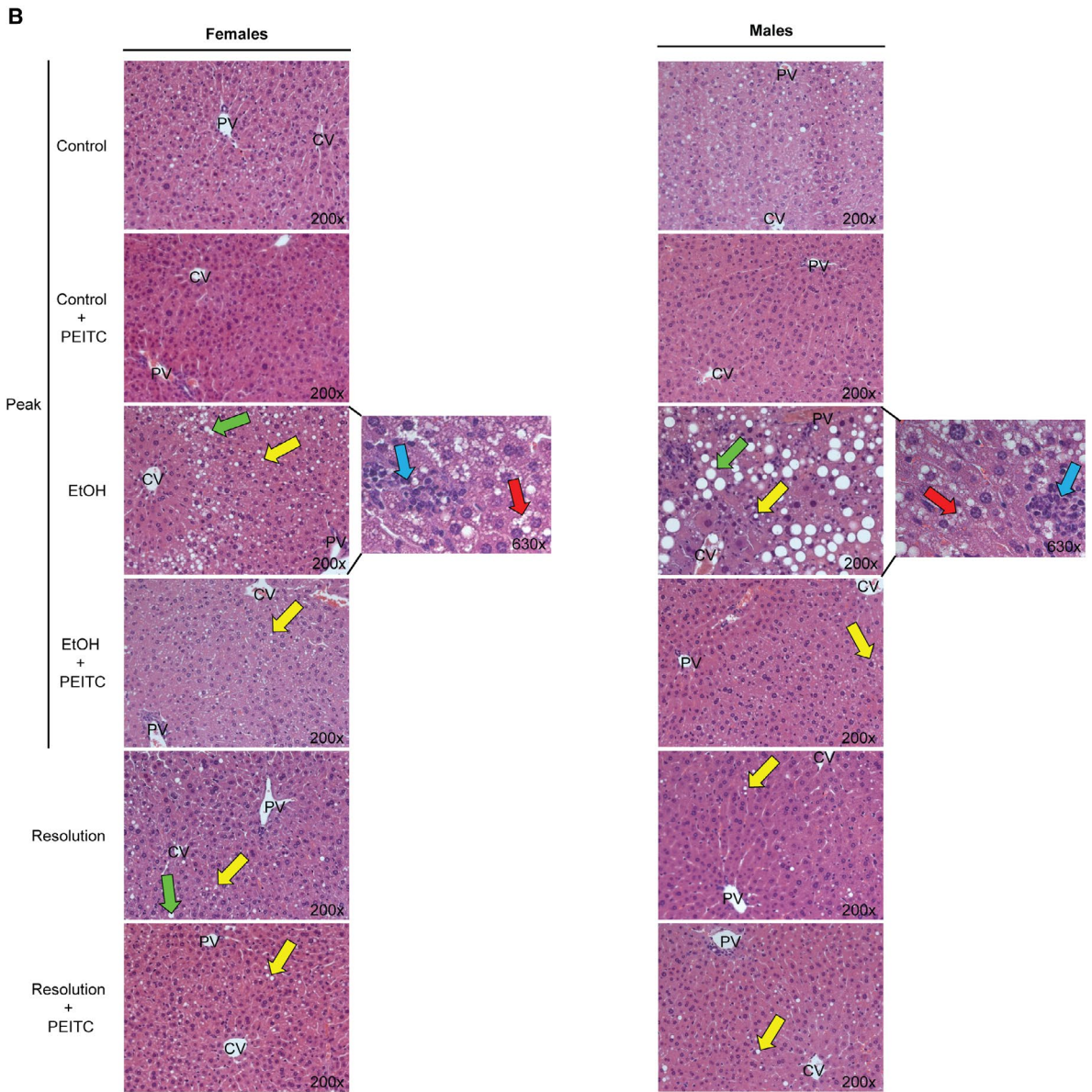
C

Parameters	Females						Males					
	Peak				Resolution	Resolution + PEITC	Peak				Resolution	Resolution + PEITC
	Control	Control + PEITC	EtOH	EtOH + PEITC			Control	Control + PEITC	EtOH	EtOH + PEITC		
Steatosis	0.5±0.3	0.25±0.2	2.0±0.4*	0.75±0.3^	0.75±0.2	0.25±0.3	0.5±0.2	0.5±0.3	2.6±0.3**	0.75±0.2^^	0.25±0.3	0.25±0.2
Inflammation	0.75±0.2	0.5±0.3	1.75±0.3*	0.75±0.3^	0.5±0.3	0.25±0.2	0.5±0.3	0.5±0.2	1.67±0.3*	0.5±0.2^	0.5±0.3	0.5±0.3
Hepatocyte ballooning	0.25±0.2	0.25±0.2	1.5±0.3*	0.57±0.3^	0.57±0.2	0.5±0.3	0.25±0.3	0.25±0.2	1.33±0.3*	0.57±0.2	0.57±0.3	0.57±0.3
Serum ALT (IU/L)	47.1±13.2	67.8±12.7	166.5±29.2*	78.5±3.2^	65.1±9.7	38.0±7.1	50.7±15.7	54.9±7.3	197.9±41.5*	75.6±8.6^	74.1±11.6	46.8±2.1

FIG. 8. Continued.

D

E

Nuclear fraction

	Control	AA	EtOH	EtOH + AA
MAP3K1				
Histone H3				
	1.0 ± 0.0	0.9 ± 0.1	3.3 ± 0.3 **ttt**	4.1 ± 0.1 **ttt**

Cytosolic fraction

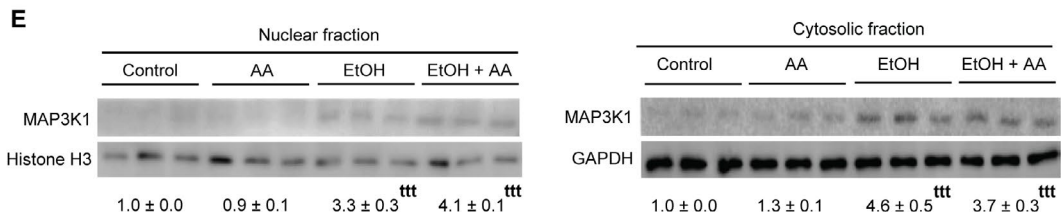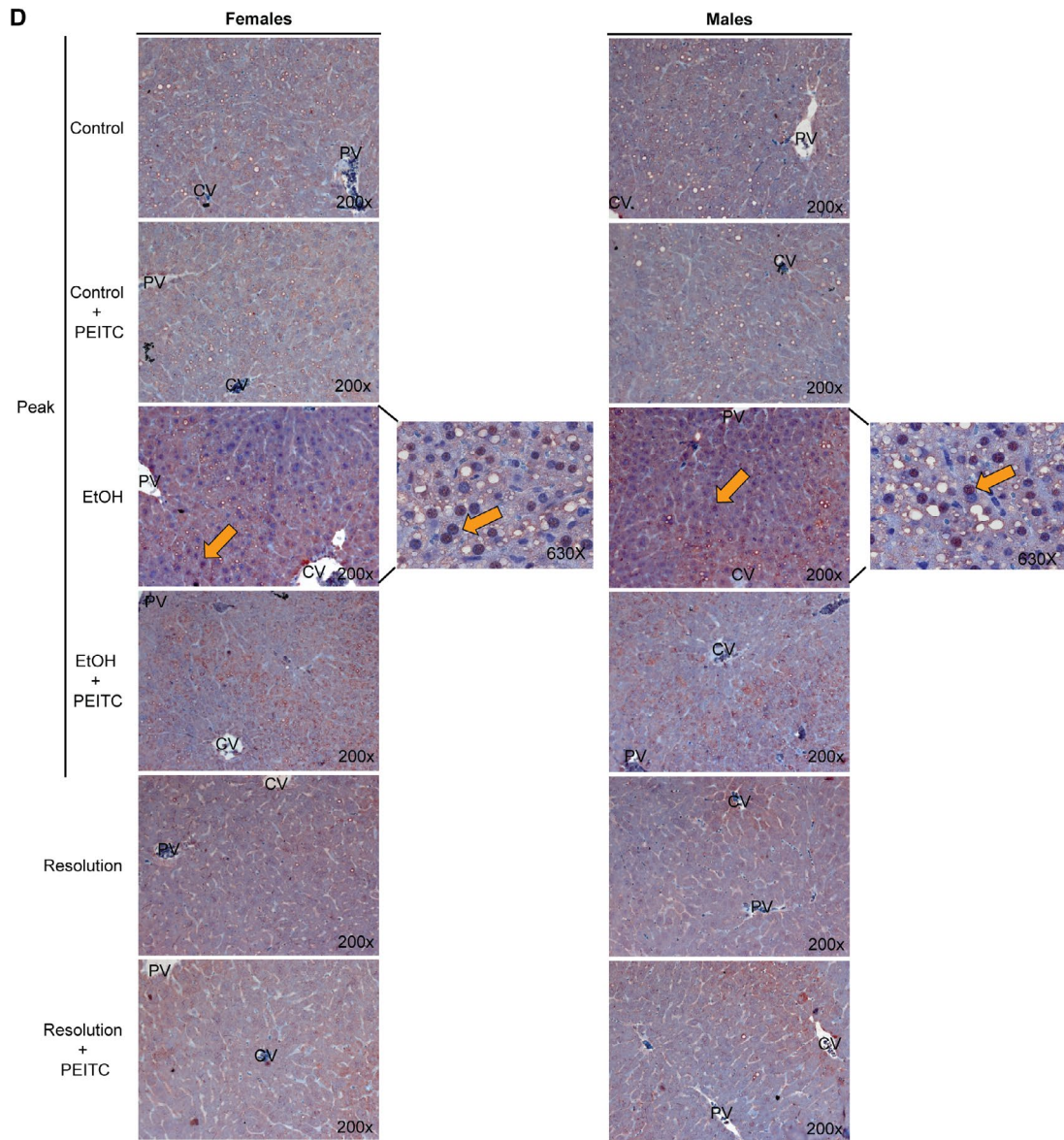|	Control	AA	EtOH	EtOH + AA
MAP3K1				
GAPDH				
	1.0 ± 0.0	1.3 ± 0.1	4.6 ± 0.5 **ttt**	3.7 ± 0.3 **ttt**

FIG. 8. Continued.

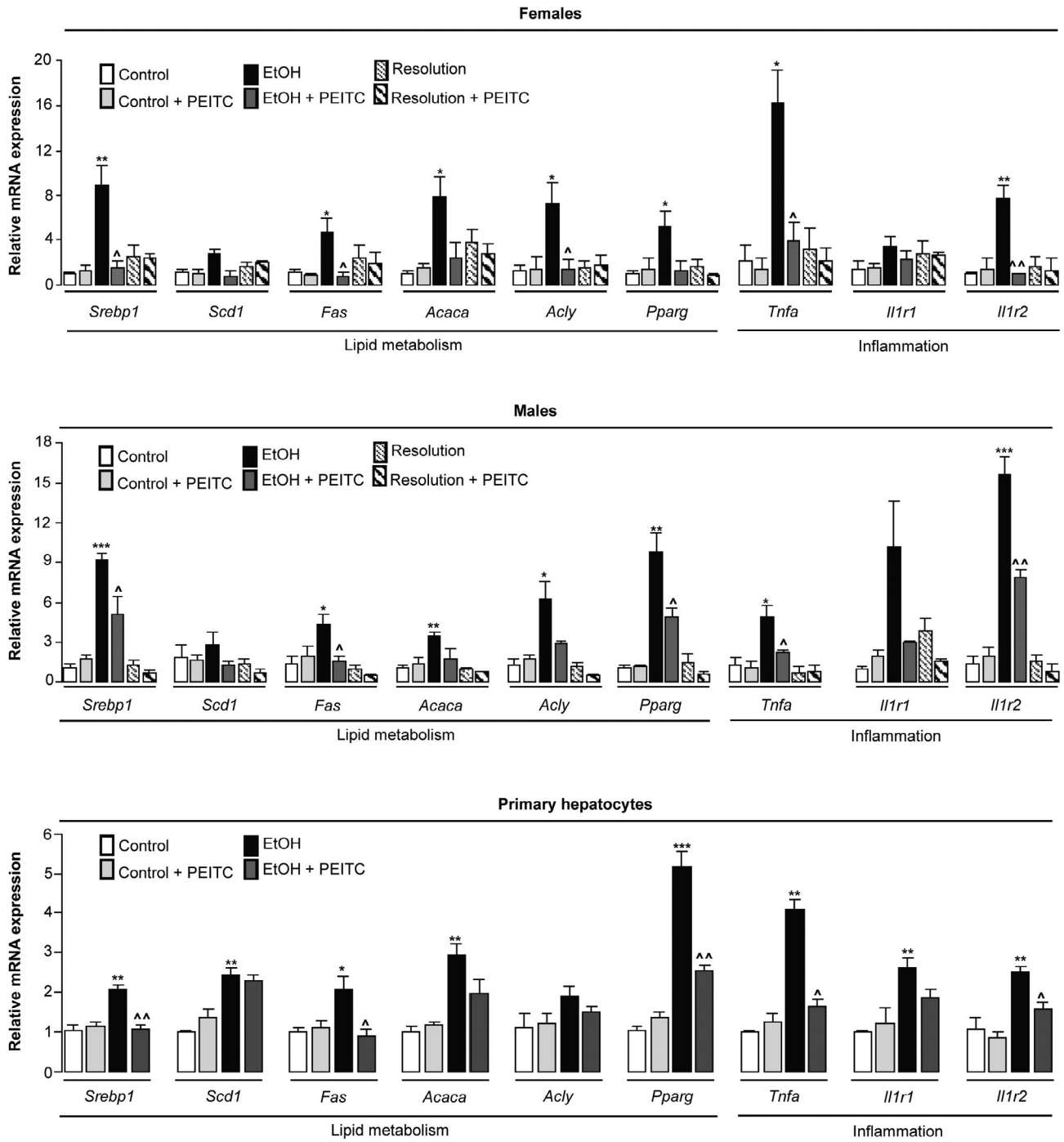**F**   Effect of Map3k1 inhibition on hepatic lipid metabolism and inflammation

FIG. 8. Continued.

Moreover, this dipeptide inhibits the uptake of a wide variety of amino acids by the small intestine,[34] suggesting that alcohol could inhibit intestinal protein synthesis. Hence, these observations indicate that alcohol could directly act on intestinal protein metabolism.

Microbiome and metabolome correlation analysis reveal a strong relationship with alteration at peak and restoration during resolution from ALD. Alcohol abstinence restores intestinal dysbiosis, and this may reinstate intestinal metabolism or *vice versa*. Correlation analysis between liver transcriptome and microbiome or metabolome shows stronger correlation between hepatic genes and bacteria than between genes and metabolites. However, a small number of genes strongly correlate with both bacteria and metabolites. Among these is *Map3k1*, a serine/threonine kinase and a signal transducer.[35] According to the Human Protein Atlas, it is widely expressed in hepatocytes. It regulates cell death, survival, migration, differentiation, tumorigenesis, cytokine production, and humoral immunity.[36] We show an increase in *Map3k1* expression in hepatocytes at peak and a decrease during resolution from ALD, suggesting that *Map3k1* could play a potential role in ALD.

Furthermore, IPA analysis confirms association of *Map3k1* with NF-κB, TLR, EGF, FGF, Rac, SAPK/JNK, APR, nuclear factor E2-related factor–oxidative stress (NRF2-OS), ROS/RNS and IL-1 signaling, all of which participate in ALD.[4,26,37] Analysis of publicly available liver microarray data[38,39] and WB demonstrate high hepatic expression of MAP3K1 in patients with AH compared to healthy individuals. This study also highlights that the increased nuclear translocation of MAP3K1 at peak decreases during resolution from ALD. Likewise, this occurred in primary hepatocytes treated with ethanol alone or in combination with AA, pointing both at induction and translocation of MAP3K1 in ALD. As demonstrated here, blocking MAP3K1 activity prevents steatosis, inflammation, and ALD.

Notably, we prove that the composition of BAs in portal serum changes from peak to resolution from ALD. Patients with AH show higher levels of total and conjugated BAs, particularly CA, glycocholic acid, TCA, glycochenodeoxycholic acid, and taurochenodeoxycholic acid in the systemic circulation.[40,41] In mice at peak injury, the same BAs increase in portal serum and return to baseline values during resolution from ALD; however, the changes were gender-specific.

Alcohol increases BA synthesis by up-regulating the expression of BA metabolism enzymes (cytochrome P450 [Cyp] 7a1, *Cyp27a1*, *Cyp8b1*, and *Baat*) and BA transporters (bile salt export pump [*Bsep*], multidrug resistance–associated protein 2 [*Mrp2*], phosphoglycolate phosphatase [*Pgp*] and apical sodium–bile acid transporter [*Asbt*]); however, our transcriptomics analysis does not show changes in the genes.

The composition of the gut microbiota is affected by BA metabolism, and the gut microbiome regulates BA synthesis.[42] Primary BAs (CA and CDCA) are synthesized in hepatocytes from CHO and are subsequently conjugated with taurine or glycine in the liver.[43] Conjugated BAs then enter the gallbladder, and after food intake are released into the duodenum.[44] Approximately 95% of these BAs are reabsorbed in the intestine and return to the liver through the portal circulation, while the remaining 5% are excreted through the feces.[42,44] Within the small intestine, the gut microbiota converts primary into secondary BAs. Deconjugation of taurine and glycine from conjugated BAs through hydrolysis produces the primary BAs CA and CDCA.[44] We show increased CA and decreased TCA in portal serum at peak injury in females, which declines during resolution from ALD. This indicates that in females, ethanol stimulates deconjugation of taurine-conjugated primary BAs in the intestine by the gut microbiota. However, in males at peak injury, CA is low and TCA is high in portal serum and decline during resolution from ALD. This suggests that in males, ethanol inhibits deconjugation of taurine-conjugated primary BAs in the intestine by the gut microbiota.

Our study has some limitations. First, we used a model of early alcohol-induced liver injury that does not fully replicate the phenotype of patients with AH, who develop fibrosis, bilirrubinostasis, and liver failure. Future studies will include the acute-on-chronic ethanol feeding model, which could provide additional clinical relevance. Second, resolution of liver injury in mice occurs faster than in humans. Third, we chose day 3 and day 14 to study early and late resolution, respectively. On day 3, most of the parameters of liver injury showed normalization, at least in males. Thus, use of earlier time points for resolution from ALD will be informative. Fourth, while the portal serum metabolome is a proxy of the fecal metabolome, it also contains some host-specific species.

In summary, the results from this study demonstrate that resolution from ALD following cessation

of alcohol drinking is mediated by restoration of the hepatic transcriptome, fecal microbiome, and portal serum metabolome, to ultimately control key molecular pathways in the liver. These events improve the crosstalk within the gut-liver axis, a major player in ALD.[8] The data indicate that alcohol drinking induces hepatic expression of MAP3K1 and abstinence returns it to baseline values. Furthermore, MAP3K1 directly correlates with most of the altered bacteria and metabolites in both genders. Therefore, alcohol directly and/or indirectly, through the gut-liver axis, drives hepatic expression of MAP3K1, which in turn contributes to progression of ALD. This may open new therapeutic opportunities to improve the clinical management of patients with ALD.

REFERENCES

1) Gao B, Bataller R. Alcoholic liver disease: pathogenesis and new therapeutic targets. Gastroenterology 2011;141:1572-1585.

2) Louvet A, Mathurin P. Alcoholic liver disease: mechanisms of injury and targeted treatment. Nat Rev Gastroenterol Hepatol 2015;12:231-242.

3) Osna NA, Donohue TM Jr, Kharbanda KK. Alcoholic liver disease: pathogenesis and current management. Alcohol Res 2017;38:147-161.

4) Pochareddy S, Edenberg HJ. Chronic alcohol exposure alters gene expression in HepG2 cells. Alcohol Clin Exp Res 2012;36:1021-1033.

5) Seth D, Leo MA, McGuinness PH, Lieber CS, Brennan Y, Williams R, et al. Gene expression profiling of alcoholic liver disease in the baboon (Papio hamadryas) and human liver. Am J Pathol 2003;163:2303-2317.

6) Sharma S, Maras JS, Das S, Hussain S, Mishra AK, Shasthry SM, et al. Pre-therapy liver transcriptome landscape in Indian and French patients with severe alcoholic hepatitis and steroid responsiveness. Sci Rep 2017;7:6816.

7) Mandrekar P, Szabo G. Signalling pathways in alcohol-induced liver inflammation. J Hepatol 2009;50:1258-1266.

8) Szabo G, Petrasek J. Gut-liver axis and sterile signals in the development of alcoholic liver disease. Alcohol Alcohol 2017;52:414-424.

9) **Gao B**, Ahmad MF, **Nagy LE**, **Tsukamoto H**. Inflammatory pathways in alcoholic steatohepatitis. J Hepatol 2019;70:249-259.

10) Schnabl B, Brenner DA. Interactions between the intestinal microbiome and liver diseases. Gastroenterology 2014;146:1513-1524.

11) Betrapally NS, Gillevet PM, Bajaj JS. Changes in the intestinal microbiome and alcoholic and nonalcoholic liver diseases: causes or effects? Gastroenterology 2016;150:1745-1755.e1743.

12) Hartmann P, Seebauer CT, Schnabl B. Alcoholic liver disease: the gut microbiome and liver cross talk. Alcohol Clin Exp Res 2015;39:763-775.

13) Sarin SK, Pande A, Schnabl B. Microbiome as a therapeutic target in alcohol-related liver disease. J Hepatol 2019;70:260-272.

14) Zhong W, Zhou Z. Alterations of the gut microbiome and metabolome in alcoholic liver disease. World J Gastrointest Pathophysiol 2014;5:514-522.

15) **Ge X**, **Antoine DJ**, Lu Y, Arriazu E, Leung T-M, Klepper AL, et al. High mobility group box-1 (HMGB1) participates in the pathogenesis of alcoholic liver disease (ALD). J Biol Chem 2014;289:22672-22691.

16) Ge X, Arriazu E, Magdaleno F, Antoine DJ, Dela Cruz R, Theise N, et al. High mobility group box-1 drives fibrosis progression signaling via the receptor for advanced glycation end products in mice. Hepatology 2018;68:2380-2404.

17) **Arriazu E**, **Ge X**, Leung T-M, Magdaleno F, Lopategi A, Lu Y, et al. Signalling via the osteopontin and high mobility group box-1 axis drives the fibrogenic response to liver injury. Gut 2017;66:1123-1137.

18) Ge X, Leung TM, Arriazu E, Lu Y, Urtasun R, Christensen B, et al. Osteopontin binding to lipopolysaccharide lowers tumor necrosis factor-alpha and prevents early alcohol-induced liver injury in mice. Hepatology 2014;59:1600-1616.

19) Cubero FJ, Nieto N. Arachidonic acid stimulates TNFalpha production in Kupffer cells via a reactive oxygen species-pERK1/2-Egr1-dependent mechanism. Am J Physiol Gastrointest Liver Physiol 2012;303:G228-G239.

20) Nieto N. Oxidative-stress and IL-6 mediate the fibrogenic effects of [corrected] Kupffer cells on stellate cells. Hepatology 2006;44:1487-1501.

21) Lieber CS, DeCarli LM. The feeding of alcohol in liquid diets: two decades of applications and 1982 update. Alcohol Clin Exp Res 1982;6:523-531.

22) Cross JV, Foss FW, Rady JM, Macdonald TL, Templeton DJ. The isothiocyanate class of bioactive nutrients covalently inhibit the MEKK1 protein kinase. BMC Cancer 2007;7:183.

23) **Wang H**, **Zhou H**, Zhang Q, Poulsen KL, Taylor V, McMullen MR, et al. Inhibition of IRAK4 kinase activity improves ethanol-induced liver injury in mice. J Hepatol 2020;73:1470-1481.

24) Shimizu I, Ito S. Protection of estrogens against the progression of chronic liver disease. Hepatol Res 2007;37:239-247.

25) Jarvelainen HA, Lukkari TA, Heinaro S, Sippel H, Lindros KO. The antiestrogen toremifene protects against alcoholic liver injury in female rats. J Hepatol 2001;35:46-52.

26) Tilg H, Moschen AR, Kaneider NC. Pathways of liver injury in alcoholic liver disease. J Hepatol 2011;55:1159-1161.

27) Horiguchi N, Wang L, Mukhopadhyay P, Park O, Jeong WI, Lafdil F, et al. Cell type-dependent pro- and anti-inflammatory role of signal transducer and activator of transcription 3 in alcoholic liver injury. Gastroenterology 2008;134:1148-1158.

28) Bhat A, Das S, Yadav G, Chaudhary S, Vyas A, Islam M, et al. Hyperoxidized albumin modulates platelets and promotes inflammation through CD36 receptor in severe alcoholic hepatitis. Hepatol Commun 2020;4:50-65.

29) Mello T, Polvani S, Galli A. Peroxisome proliferator-activated receptor and retinoic X receptor in alcoholic liver disease. PPAR Res 2009;2009:748174.

30) Gyamfi MA, Kocsis MG, He L, Dai G, Mendy AJ, Wan YJ. The role of retinoid X receptor alpha in regulating alcohol metabolism. J Pharmacol Exp Ther 2006;319:360-368.

31) Gyamfi MA, He L, French SW, Damjanov I, Wan YJY. Hepatocyte retinoid X receptor alpha-dependent regulation of lipid homeostasis and inflammatory cytokine expression contributes to alcohol-induced liver injury. J Pharmacol Exp Ther 2008;324:443-453.

32) Parker BJ, Wearsch PA, Veloo ACM, Rodriguez-Palacios A. The genus Alistipes: gut bacteria with emerging implications to inflammation, cancer, and mental health. Front Immunol 2020;11:906.

33) Bishehsari F, Magno E, Swanson G, Desai V, Voigt RM, Forsyth CB, et al. Alcohol and gut-derived inflammation. Alcohol Res 2017;38:163-171.

34) Ganapathy V, Radhakrishnan AN. Interaction of amino acids with glycyl-L-leucine hydrolysis and transport in monkey small intestine. Clin Sci 1979;57:521-527.

35) **Pham TT**, **Angus SP**, Johnson GL. MAP3K1: genomic alterations in cancer and function in promoting cell survival or apoptosis. Genes Cancer 2013;4:419-426.

36) Suddason T, Gallagher E. A RING to rule them all? Insights into the Map3k1 PHD motif provide a new mechanistic understanding into the diverse roles of Map3k1. Cell Death Differ 2015;22:540-548.

37) Beier JI, McClain CJ. Mechanisms and cell signaling in alcoholic liver disease. Biol Chem 2010;391:1249-1264.

38) **Affò S**, **Dominguez M**, Lozano JJ, Sancho-Bru P, Rodrigo-Torres D, Morales-Ibanez O, et al. Transcriptome analysis identifies TNF superfamily receptors as potential therapeutic targets in alcoholic hepatitis. Gut 2013;62:452-460.

39) Hyun J, Sun Z, Ahmadi AR, Bangru S, Chembazhi UV, Du K, et al. Epithelial splicing regulatory protein 2-mediated alternative splicing reprograms hepatocytes in severe alcoholic hepatitis. J Clin Invest 2020;130:2129-2145.

40) Ciocan D, Voican CS, Wrzosek L, Hugot C, Rainteau D, Humbert L, et al. Bile acid homeostasis and intestinal dysbiosis in alcoholic hepatitis. Aliment Pharmacol Ther 2018;48:961-974.

41) **Brandl K**, **Hartmann P**, Jih LJ, Pizzo DP, Argemi J, Ventura-Cots M, et al. Dysregulation of serum bile acids and FGF19 in alcoholic hepatitis. J Hepatol 2018;69:396-405.

42) Jia ET, Liu ZY, Pan M, Lu JF, Ge QY. Regulation of bile acid metabolism-related signaling pathways by gut microbiota in diseases. J Zhejiang Univ Sci B 2019;20:781-792.

43) Russell DW. The enzymes, regulation, and genetics of bile acid synthesis. Annu Rev Biochem 2003;72:137-174.

44) Mullish BH, Pechlivanis A, Barker GF, Thursz MR, Marchesi JR, McDonald JAK. Functional microbiomics: evaluation of gut microbiota-bile acid metabolism interactions in health and disease. Methods 2018;149:49-58.

Author names in bold designate shared co-first authorship.

Supporting Information

Additional Supporting Information may be found at onlinelibrary.wiley.com/doi/10.1002/hep4.1793/suppinfo.